The discontinuous enrichment method

Charbel Farhat [a,1], Isaac Harari [b,2], Leopoldo P. Franca [c]

[a]*Department of Aerospace Engineering Sciences, University of Colorado at Boulder, Boulder, CO 80309-0429, USA*

[b]*Department of Solid Mechanics, Materials, and Systems, Tel Aviv University, 69978 Ramat Aviv, ISRAEL*

[c]*Department of Mathematics, University of Colorado at Denver, Denver, CO 80217-3364, USA*

Abstract

We propose a finite element based discretization method in which the standard polynomial field is enriched within each element by a nonconforming field that is added to it. The enrichment contains free-space solutions of the homogeneous differential equation that are not represented by the underlying polynomial field. Continuity of the enrichment across element interfaces is enforced weakly by Lagrange multipliers. In this manner, we expect to attain high coarse-mesh accuracy without significant degradation of conditioning, assuring good performance of the computation at any mesh resolution. Examples of application to acoustics and advection-diffusion are presented.

Key words: Finite elements; discontinuous enrichment; acoustics; advection-diffusion

1 Introduction

The standard finite element method is based on continuous, piecewise polynomial, Galerkin approximation. This approach is optimal for the Laplace operator in the sense that it minimizes the error in the energy norm—the H^1 semi-norm in this case. This property assures good performance of the computation at any mesh resolution, i.e., high coarse-mesh accuracy. However, good numerical performance at any mesh resolution is not guaranteed

---

[1] Corresponding author; e-mail: charbel.farhat@colorado.edu.
[2] This work was done while the author was visiting the University of Colorado at Boulder.

by the standard finite element method for other cases. Consequently, finite element computation can become prohibitively expensive in the presence of sharp gradients and rapid oscillations.

Numerous approaches to alleviating the above deficiency have been proposed. Inevitably, these are based on modifications of the classical piecewise polynomial Galerkin approximation. Among these approaches we note Galerkin/least-squares [43] and related stabilized methods (SUPG/SD [18] and USFEM [35]), residual-free bubbles (RFB) [17, 34, 36, 37], variational multiscale (VMS) [40], the partition of unity method (PUM) [5, 49], and nearly optimal Petrov-Galerkin [7]. More special-purpose approaches include the quasi-stabilized method [4, 6], finite increment calculus [50], subgrid modeling [21], and the residual-based method proposed in [51]. Relationships between some of these approaches have been established and described in [16, 32, 33].

For the Helmholtz equation, PUM provides very accurate results at low wave resolutions, but suffers from severe ill-conditioning that renders the method ineffective in practice. (It is still unclear whether a current implementation of PUM for acoustic waves [47] can circumvent this difficulty.)

Motivated by PUM, RFB, the FETI method for nonconforming domain decomposition with Lagrange multipliers [24, 25, 29, 31], and recent work on discontinuous Galerkin methods (DGM) for second-order equations [3, 8, 9, 52], we propose herein a discretization method in which the standard finite element polynomial field within each element is enriched by free-space solutions of the governing homogeneous, constant-coefficient, partial differential equation. These enrichments are easy to obtain, and are virtually independent of element geometry and polynomial order. Thus, features of the differential equation are included in the approximation. Like PUM, the number of such homogeneous solutions is determined in advance. Like RFB, but in contrast to PUM, the enrichment is *added* to, rather than multiplied by, the polynomial field. Consequently, the enrichment field is not continuous across element boundaries ab initio, and continuity is enforced weakly by Lagrange multipliers. In this manner, we expect to retain the high coarse-mesh accuracy of PUM, without significant degradation of conditioning. As in the DGM work cited above, we address a second-order partial differential equation directly rather than cast it as a first-order system. We also note that the enrichment being spanned by free-space solutions that are discontinuous across element boundaries, as proposed, is reminiscent of Trefftz approximations [19, 45, 46, 56].

The concept of finite element methods with Lagrange multipliers for enforcing boundary constraints is well known [2]. It has been successfully applied to the analysis of structural systems modeled by different types of elements [53], to the investigation of contact problems [55], to the synthesis of independently discretized subdomains and modeled substructures [1, 10, 26, 27], and to the

design of fast, domain decomposition based, iterative solvers [24, 30, 31].

The remainder of this paper is organized as follows. The Discontinuous Enrichment Method (DEM) is presented in Sec. 2 as a general approach for improving finite element computation. Implementational issues related to static condensation of the enrichment field, approximation of Lagrange multipliers, treatment of Neumann and Robin boundary conditions, as well as numerical integration are outlined in Sec. 3. The application of DEM to the Helmholtz equation is described in Sec. 4, with suggested approximations, dispersion analyses, and numerical tests. Advection-diffusion is treated similarly in Sec. 5. Conclusions are offered in Sec. 6.

2 The Discontinuous Enrichment Method for an Abstract Dirichlet Problem

Let $\Omega \subset \mathbb{R}^d$ be a d-dimensional, open, bounded region with smooth boundary Γ. For simplicity, we consider the following Dirichlet boundary-value problem: find $u : \overline{\Omega} \to \mathbb{R}$ such that

$$\mathcal{L}u = f \qquad \text{in } \Omega \tag{1}$$
$$u = g \qquad \text{on } \Gamma \tag{2}$$

Here, $f : \Omega \to \mathbb{R}$ and $g : \Gamma \to \mathbb{R}$ are given functions. We think of $\mathcal{L}$ as a second-order differential operator. The method proposed herein may be generalized to problems with other types of boundary conditions (see Sec. 3.3).

Partition Ω into n_{el} nonoverlapping regions Ω^e (element domains) with boundaries Γ^e (Fig. 1), $e = 1, \ldots n_{\text{el}}$, i.e.,

$$\overline{\Omega} = \overline{\bigcup_{e=1}^{n_{\text{el}}} \Omega^e} \tag{3}$$

where

$$\bigcap_{e=1}^{n_{\text{el}}} \Omega^e = \emptyset \tag{4}$$

We denote the union of element interiors by

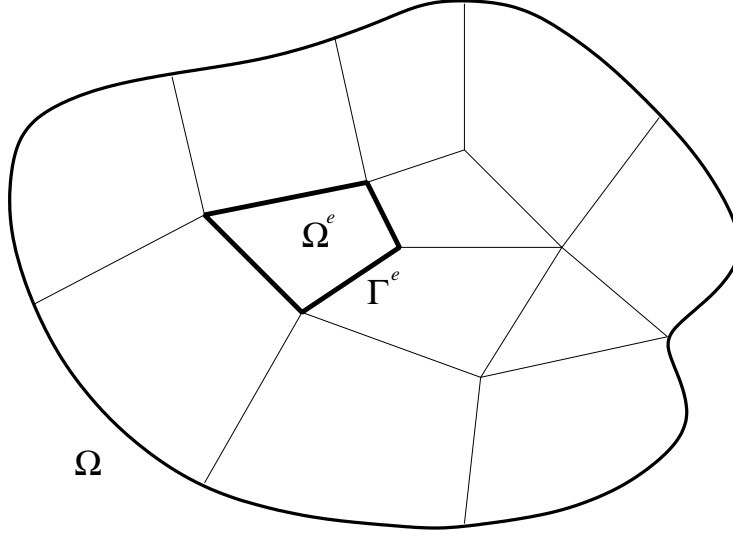$$\widetilde{\Omega} = \bigcup_{e=1}^{n_{\text{el}}} \Omega^e \tag{5}$$

3

Fig. 1. Domain Ω partitioned into element domains Ω^e.

Similarly, the union of element boundaries is denoted

$$\widetilde{\Gamma} = \bigcup_{e=1}^{n_{\mathrm{el}}} \Gamma^e \tag{6}$$

The element interfaces or interior element boundaries are

$$\Gamma_{\mathrm{int}} = \widetilde{\Gamma} \setminus \Gamma \tag{7}$$

2.1 Hybrid variational formulation with weak continuity

The variational form of the boundary-value problem (1)–(2) is stated in terms of the set of trial solutions $\mathcal{V} = L_2(\Omega) \cap H^1\left(\widetilde{\Omega}\right)$. These functions may be discontinuous across element boundaries. Similarly, the functions are not required to satisfy Dirichlet boundary conditions.

Inter-element continuity and Dirichlet boundary conditions are both enforced weakly by Lagrange multipliers in $H^{-1/2}\left(\widetilde{\Gamma}\right)$. Following a procedure outlined in [15, Sec. I.4], we introduce $\boldsymbol{p} \in \mathcal{W} = H\left(\mathrm{div}; \Omega\right)$, where

$$H\left(\mathrm{div}; \Omega\right) = \left\{\boldsymbol{p} \mid \boldsymbol{p} \in (L_2(\Omega))^d, \ \mathrm{div}\boldsymbol{p} \in L_2(\Omega)\right\} \tag{8}$$

The normal traces of $\boldsymbol{p}$ on Γ^e are taken as Lagrange multipliers. These well-defined normal traces $\boldsymbol{p} \cdot \boldsymbol{n}$ lie in $H^{-1/2}\left(\widetilde{\Gamma}\right)$ [48, 57] and satisfy

$$\langle \boldsymbol{p} \cdot \boldsymbol{n}, v \rangle_{\Gamma^e} = (\nabla v, \boldsymbol{p})_{\Omega^e} + (v, \mathrm{div}\boldsymbol{p})_{\Omega^e} \tag{9}$$

4

Here, $\langle \cdot, \cdot \rangle$ is the duality pairing between $H^{-1/2}(\Gamma)$ and $H^{1/2}(\Gamma)$, and $(\cdot, \cdot)$ is the $L_2(\Omega)$ inner product. Subscripts on duality pairings denote domains of integration other than Γ, and subscripts on inner products denote domains of integration other than Ω. The outward unit vector normal to a boundary is denoted by $\boldsymbol{n}$. No additional degrees of freedom are required in the approximation of the Lagrange multipliers as the normal traces of $\boldsymbol{p}$, compared to scalar functions defined over element boundaries (see Sec. 3.2 for more details and examples of approximations of $\boldsymbol{p}$).

We now seek the stationary point $u \in \mathcal{V}$ and $\boldsymbol{p} \in \mathcal{W}$ of the Lagrangian

$$\Pi(u, \boldsymbol{p}) = \frac{1}{2} \, a(u, u) - \langle \boldsymbol{p} \cdot \boldsymbol{n}, u \rangle_{\widetilde{\Gamma}} - L(u) - L_{\mathrm{b}}(\boldsymbol{p}) \tag{10}$$

Allowing for discontinuities, the bilinear operator $a(\cdot, \cdot)$ is defined over element interiors $\widetilde{\Omega}$, satisfying

$$a(v, u) = (v, \mathcal{L}u)_{\widetilde{\Omega}} + \langle \mathcal{L}_{\mathrm{b}} u, v \rangle_{\widetilde{\Gamma}} \tag{11}$$

Here, $\mathcal{L}_{\mathrm{b}}$ is the boundary operator corresponding to $\mathcal{L}$. Terms representing the data are

$$L(v) = (v, f) \tag{12}$$
$$L_{\mathrm{b}}(\boldsymbol{q}) = - \langle \boldsymbol{q} \cdot \boldsymbol{n}, g \rangle \tag{13}$$

for sufficiently smooth f and g.

Several stabilized methods include jumps involving the boundary operator across element interfaces [22, 42, 44, 51]. Such terms are derived directly from the governing equations in VMS [41]. The present formulation enforces continuity of the field itself. These terms are employed to obtain a local approximation of the global effect of phenomena unresolved by the mesh.

2.2 *Weak form*

The stationary point of the functional (10) is obtained by setting its first variation to zero. In partitioned form, this leads to

$$a(v, u) - \langle \boldsymbol{p} \cdot \boldsymbol{n}, v \rangle_{\widetilde{\Gamma}} = L(v) \tag{14}$$
$$- \langle \boldsymbol{q} \cdot \boldsymbol{n}, u \rangle_{\widetilde{\Gamma}} = L_{\mathrm{b}}(\boldsymbol{q}) \tag{15}$$

Here, $v \in \mathcal{V}$ and $\boldsymbol{q} \in \mathcal{W}$ are arbitrary variations of u and $\boldsymbol{p}$, respectively.

The key stability condition for mixed and hybrid formulations is the Babuška-Brezzi (inf-sup) condition (e.g., [15, p. 57]) governing the selection of finite element interpolations. Discretization of (14) and (15) leads to a typical 'zero' diagonal block [15, p. 74].

The corresponding Euler-Lagrange equations are

$$\mathcal{L}u = f \qquad \text{in } \widetilde{\Omega} \tag{16}$$
$$[\![u]\!] = 0 \qquad \text{on } \Gamma_{\text{int}} \tag{17}$$
$$u = g \qquad \text{on } \Gamma \tag{18}$$
$$\boldsymbol{p} \cdot \boldsymbol{n} = \mathcal{L}_{\text{b}}u \quad \text{on } \widetilde{\Gamma} \tag{19}$$

Here, $[\![\cdot]\!]$ is the jump at an element boundary. Equation (19) provides an interpretation of the Lagrange multiplier. For example, if $\mathcal{L}_{\text{b}}$ is the normal derivative, then $\boldsymbol{p} = \nabla u$ in $\widetilde{\Omega}$.

2.3 Galerkin approximation

We seek approximate solutions $u^h \in \mathcal{V}^h \subset \mathcal{V}$ of the form

$$u^h = u^{\text{P}} + u^{\text{E}} \tag{20}$$

Here, $u^{\text{P}} \in \mathcal{V}^{\text{P}} \subset H^1(\Omega)$ are standard, continuous, piecewise polynomial, finite element functions—the coarse scales in variational multiscale terminology, and $u^{\text{E}} \in \mathcal{V}^{\text{E}}$ is the enrichment field. Unlike the fine scales or bubbles, which fill a similar role, u^{E} may be discontinuous across element boundaries. This allows us to circumvent both the difficulty in attempting to approximate the global fine-scale Green's function of the variational multiscale method, and the loss of global effects due to the restriction of residual-free bubbles to a vanishing trace on element boundaries. An added potential benefit is improved approximation of discontinuous solutions.

There is a great deal of flexibility in selecting $\mathcal{V}^{\text{E}}$ in this framework. We assume that the approximation of particular solutions by $\mathcal{V}^{\text{P}}$ is satisfactory. The enrichment should therefore contain solutions of the homogeneous partial differential equation that are not represented by the underlying polynomial field, a.k.a. the fine scales. We note that this interpretation of the fine scales differs somewhat from that of VMS or RFB. In the present method, the enrichment field may entirely capture homogeneous solutions, rather than merely enhance the polynomial field.

Weak enforcement of continuity permits the use of free-space solutions as bases for the enrichment. Consequently, potentially difficult, element-level

boundary-value problems need not be solved, neither analytically nor numerically. The relatively simple, free-space solutions are applicable to practically any element polynomial order and geometry.

In summary, we employ the direct sum relationship $\mathcal{V}^h = \mathcal{V}^{\mathrm{P}} \oplus \mathcal{V}^{\mathrm{E}}$, where $u^{\mathrm{E}} \in \mathcal{V}^{\mathrm{E}}$ and $\mathcal{V}^{\mathrm{E}}$ is spanned by solutions of

$$\mathcal{L}u^{\mathrm{E}} = 0 \qquad \text{in } \mathbb{R}^d \tag{21}$$

that are not already represented in the polynomial basis. Since these functions are employed on an element level, we typically employ solutions of the constant-coefficient case, which are easy to obtain.

The approximation of the Lagrange multipliers as normal traces of a vector-valued function on element boundaries is well-established from previous work on hybrid methods (see [15, Sec. III.3] for an extensive discussion of definitions of $\mathcal{W}^h \subset \mathcal{W}$). Implementational issues are outlined in Sec. 3.2.

The treatment of weighting functions is consistent with Eqn. (20), namely, $v^h = v^{\mathrm{P}} + v^{\mathrm{E}} \in \mathcal{V}^h$ and $\boldsymbol{q}^h \in \mathcal{W}^h$. By the Galerkin method, we seek $u^h \in \mathcal{V}^h$ and $\boldsymbol{p}^h \in \mathcal{W}^h$ such that $\forall \left\{ v^h, \boldsymbol{q}^h \right\} \in \mathcal{V}^h \times \mathcal{W}^h$

$$a(v^h, u^h) - \left\langle \boldsymbol{p}^h \cdot \boldsymbol{n}, v^h \right\rangle_{\widetilde{\Gamma}} = L(v^h) \tag{22}$$

$$-\left\langle \boldsymbol{q}^h \cdot \boldsymbol{n}, u^h \right\rangle_{\widetilde{\Gamma}} \hspace{2.2cm} = L_{\mathrm{b}}(\boldsymbol{q}^h) \tag{23}$$

These equations may be decomposed as follows

$$a(v^{\mathrm{P}}, u^{\mathrm{P}}) + a(v^{\mathrm{P}}, u^{\mathrm{E}}) - \left\langle \boldsymbol{p}^h \cdot \boldsymbol{n}, v^{\mathrm{P}} \right\rangle = L(v^{\mathrm{P}}) \tag{24}$$

$$a(v^{\mathrm{E}}, u^{\mathrm{P}}) + a(v^{\mathrm{E}}, u^{\mathrm{E}}) - \left\langle \boldsymbol{p}^h \cdot \boldsymbol{n}, v^{\mathrm{E}} \right\rangle_{\widetilde{\Gamma}} = L(v^{\mathrm{E}}) \tag{25}$$

$$-\left\langle \boldsymbol{q}^h \cdot \boldsymbol{n}, u^{\mathrm{P}} \right\rangle - \left\langle \boldsymbol{q}^h \cdot \boldsymbol{n}, u^{\mathrm{E}} \right\rangle_{\widetilde{\Gamma}} \hspace{1.2cm} = L_{\mathrm{b}}(\boldsymbol{q}^h) \tag{26}$$

Due to the discontinuous nature of $\mathcal{V}^{\mathrm{E}}$, Eqn. (25) may be used to eliminate u^{E} by static condensation on the *element* level (see Secs. 3.1 and 5.1). This procedure provides a local (and hence economical) approximation of the global effect of the fine scales on the coarse scales. The fine scales are driven by the inner-element residuals $L(v^{\mathrm{E}}) - a(v^{\mathrm{E}}, u^{\mathrm{P}})$, and the inter-element and boundary discontinuities $\left\langle \boldsymbol{p}^h \cdot \boldsymbol{n}, v^{\mathrm{E}} \right\rangle_{\widetilde{\Gamma}}$. The discontinuous terms approximate the global nature of this effect at the cost of employing additional degrees of freedom. On the other hand, once the problem has been solved, the auxiliary field directly provides accurate (and continuous) gradient information at no added cost. For example, if $\mathcal{L}_{\mathrm{b}}$ is the normal derivative, then $\boldsymbol{p}^h$ approximates ∇u in $\widetilde{\Omega}$, see Euler-Lagrange equation (19).

3 Implementation

3.1 Static condensation

More than merely a conceptual device, the local elimination of u^{E}, leading to a u^{P}-$\boldsymbol{p}$ formulation, is proposed as a *practical* procedure that simplifies and conditions the formulation, in order to reduce computational cost. Thus, the cost of solving the matrix problem that ensues from DEM is virtually independent of the dimension of u^{E}. (This holds for fully efficient sparse solvers even without static condensation.)

The enrichment field generally contains several degrees of freedom in each element. Consequently, static condensation is presented in this section in terms of the discrete equations for simplicity. For advection-diffusion the enrichment may contain a single degree of freedom. Static condensation in terms of continuous operators for this case is presented in Sec. 5.1.

Consider a partitioned form of the global system of discrete equations

$$
\begin{bmatrix} \mathbf{K}^{\mathrm{PP}} & \mathbf{K}^{\mathrm{PE}} & \mathbf{K}^{\mathrm{PC}} \\ \mathbf{K}^{\mathrm{EP}} & \mathbf{K}^{\mathrm{EE}} & \mathbf{K}^{\mathrm{EC}} \\ \mathbf{K}^{\mathrm{CP}} & \mathbf{K}^{\mathrm{CE}} & \mathbf{0} \end{bmatrix} \begin{Bmatrix} \mathbf{u}^{\mathrm{P}} \\ \mathbf{u}^{\mathrm{E}} \\ \mathbf{p} \end{Bmatrix} = \begin{Bmatrix} \mathbf{F}^{\mathrm{P}} \\ \mathbf{F}^{\mathrm{E}} \\ \mathbf{F}^{\mathrm{C}} \end{Bmatrix} \tag{27}
$$

Here, $\mathbf{u}^{\mathrm{P}}$, $\mathbf{u}^{\mathrm{E}}$, and $\mathbf{p}$ are vectors containing the degrees of freedom of u^{P}, u^{E}, and $\boldsymbol{p}^{h}$, respectively. The matrices in (27) emanate from terms in the Galerkin equations according to the correspondence outlined in Table 1. Due to the continuity of u^{P}, the arrays $\mathbf{K}^{\mathrm{PC}}$ and $\mathbf{K}^{\mathrm{CP}}$ are empty except along the domain boundary Γ.

The global system is obtained from an assembly of element arrays. Assembly of the nodal polynomial degrees of freedom is conventional. The coefficients of the enrichment are generalized degrees of freedom, internal to each element. The constraint degrees of freedom are defined on element boundaries: vertices, edges, and faces in one, two, and three dimensions, respectively. The element array is

$$
\mathbf{k}^{e} = \begin{bmatrix} \mathbf{k}^{\mathrm{PP}} & \mathbf{k}^{\mathrm{PE}} & \mathbf{k}^{\mathrm{PC}} \\ \mathbf{k}^{\mathrm{EP}} & \mathbf{k}^{\mathrm{EE}} & \mathbf{k}^{\mathrm{EC}} \\ \mathbf{k}^{\mathrm{CP}} & \mathbf{k}^{\mathrm{CE}} & \mathbf{0} \end{bmatrix} \tag{28}
$$

8

Table 1
Correspondence between the global matrices in (27) and terms in the Galerkin equations.

Matrix	Galerkin term
$\mathbf{K}^{\mathrm{PP}}$	$a(v^{\mathrm{P}}, u^{\mathrm{P}})$
$\mathbf{K}^{\mathrm{PE}}$	$a(v^{\mathrm{P}}, u^{\mathrm{E}})$
$\mathbf{K}^{\mathrm{PC}}$	$-\left\langle \boldsymbol{p}^h \cdot \boldsymbol{n}, v^{\mathrm{P}} \right\rangle$
$\mathbf{K}^{\mathrm{EP}}$	$a(v^{\mathrm{E}}, u^{\mathrm{P}})$
$\mathbf{K}^{\mathrm{EE}}$	$a(v^{\mathrm{E}}, u^{\mathrm{E}})$
$\mathbf{K}^{\mathrm{EC}}$	$-\left\langle \boldsymbol{p}^h \cdot \boldsymbol{n}, v^{\mathrm{E}} \right\rangle_{\widetilde{\Gamma}}$
$\mathbf{K}^{\mathrm{CP}}$	$-\left\langle \boldsymbol{q}^h \cdot \boldsymbol{n}, u^{\mathrm{P}} \right\rangle$
$\mathbf{K}^{\mathrm{CE}}$	$-\left\langle \boldsymbol{q}^h \cdot \boldsymbol{n}, u^{\mathrm{E}} \right\rangle_{\widetilde{\Gamma}}$
$\mathbf{F}^{\mathrm{P}}$	$L(v^{\mathrm{P}})$
$\mathbf{F}^{\mathrm{E}}$	$L(v^{\mathrm{E}})$
$\mathbf{F}^{\mathrm{C}}$	$L_{\mathrm{b}}(\boldsymbol{q}^h)$

with the obvious correspondence between global and element matrices. Note that for optimal results of the following procedure on the element level, the terms emanating from $\left\langle \boldsymbol{p}^h \cdot \boldsymbol{n}, v^{\mathrm{P}} \right\rangle_{\Gamma^e}$ and $\left\langle \boldsymbol{q}^h \cdot \boldsymbol{n}, u^{\mathrm{P}} \right\rangle_{\Gamma^e}$ should be retained in $\mathbf{k}^{\mathrm{PC}}$ and $\mathbf{k}^{\mathrm{CP}}$, respectively, although in assembly they cancel out everywhere except along the domain boundary.

The enrichment degrees of freedom are eliminated on the element level to obtain

$$\tilde{\mathbf{k}}^e = \begin{bmatrix} \tilde{\mathbf{k}}^{\mathrm{PP}} & \tilde{\mathbf{k}}^{\mathrm{PC}} \\ \tilde{\mathbf{k}}^{\mathrm{CP}} & \tilde{\mathbf{k}}^{\mathrm{CC}} \end{bmatrix} \tag{29}$$

where

$$\tilde{\mathbf{k}}^{\mathrm{PP}} = \mathbf{k}^{\mathrm{PP}} - \mathbf{k}^{\mathrm{PE}} \left(\mathbf{k}^{\mathrm{EE}} \right)^{-1} \mathbf{k}^{\mathrm{EP}} \tag{30}$$

$$\tilde{\mathbf{k}}^{\mathrm{PC}} = \mathbf{k}^{\mathrm{PC}} - \mathbf{k}^{\mathrm{PE}} \left(\mathbf{k}^{\mathrm{EE}} \right)^{-1} \mathbf{k}^{\mathrm{EC}} \tag{31}$$

$$\tilde{\mathbf{k}}^{\mathrm{CP}} = \mathbf{k}^{\mathrm{CP}} - \mathbf{k}^{\mathrm{CE}} \left(\mathbf{k}^{\mathrm{EE}} \right)^{-1} \mathbf{k}^{\mathrm{EP}} \tag{32}$$

$$\tilde{\mathbf{k}}^{\mathrm{CC}} = \qquad - \mathbf{k}^{\mathrm{CE}} \left(\mathbf{k}^{\mathrm{EE}} \right)^{-1} \mathbf{k}^{\mathrm{EC}} \tag{33}$$

Static condensation eliminates the zero diagonal block of the uncondensed matrix.

The global system for the resulting, reduced u^{P}-$\boldsymbol{p}$ formulation is obtained as an assembly of the element arrays. This system is particularly well suited for iterative solution. (Results of preliminary numerical studies of the conditioning of the coefficient matrices are favorable, see Sec. 4.) The solution for the eliminated field is then obtained as a post process within each element.

3.2 Approximation of the Lagrange multipliers

An extensive survey of techniques for approximating Lagrange multipliers of the form employed herein, including references, theoretical results, constructions of discretizations, and examples of families of elements, is presented in [15, Sec. III.3] for two- and three-dimensional configurations.

Our only departure from the presentation of [15] is a scaling of the Lagrange multiplier basis functions by a scaling factor s with the dimension of $\mathcal{L}_{\mathrm{b}}$. For a given $\mathcal{L}$, s is chosen so that the entries in the coefficient matrices corresponding to $\boldsymbol{p}$ and u are of the same order of magnitude, in order to improve the conditioning of the matrix equations. In the following we highlight a few specific examples of the approximation of Lagrange multipliers in two dimensions.

Consider Lagrange multipliers that are *constant* along the sides of a triangle. This is obtained in the present approach as normal traces of

$$\boldsymbol{p}^h(x,y) = s \left\{ \begin{array}{c} c_1 + c_3 x \\ c_2 + c_3 y \end{array} \right\}, \qquad (x,y) \in \Omega^e \tag{34}$$

on the sides of the triangle [54], originally denoted RT_0. In this case $\mathrm{div}\boldsymbol{p}^h = $ const. in Ω^e. Let (x_a, y_a) and (x_b, y_b) be the coordinates of two vertices defining a side of the triangle. The normal is

$$\boldsymbol{n}^h = \frac{\pm 1}{l} \left\{ \begin{array}{c} y_b - y_a \\ x_a - x_b \end{array} \right\} \tag{35}$$

where $l = \sqrt{(x_b - x_a)^2 + (y_b - y_a)^2}$ is the length of the side. On this side

$$\boldsymbol{p}^h \cdot \boldsymbol{n} = \pm s \left(-c_1(y_b - y_a) + c_2(x_b - x_a) + c_3(y_a x_b - x_a y_b) \right)/l \tag{36}$$

Clearly, the normal trace is constant as required, and the approximation can be specified by the three normal components of $\boldsymbol{p}^h$ on the boundary, i.e., c_1, c_2, and c_3 can be expressed in terms of the three edge values of $\boldsymbol{p}^h \cdot \boldsymbol{n}$.

A triangle with Lagrange multipliers that vary linearly along its sides, denoted BDM_1 [14], is obtained by considering nodes at the three vertices, with standard linear interpolation of nodal values of $\boldsymbol{p}^h$. The six nodal degrees of freedom of this element may be replaced by six normal components of $\boldsymbol{p}^h$ on Γ^e (two per side). However, the nodal representation is particularly well-suited for conventional finite element data structures, and if $\boldsymbol{p}^h$ is taken as $C^0\left(\widetilde{\Omega}\right)$, standard assembly procedures may be employed.

Approximations for quadrilaterals are defined in terms of natural coordinates in a square reference domain that is aligned with the axes. In case the approximation is specified in terms of the normal components on the element sides, the mapping to the the physical domain is performed by the change of variables known as Piola's transformation [15, p. 97] so that the normal components are preserved. Otherwise, when nodal values are used in conjunction with integration according to the right-hand side of (9), standard isoparametric mapping may be employed.

Consider Lagrange multipliers that are *constant* along the sides of a square reference domain. This is obtained in the present approach as normal traces of

$$\boldsymbol{p}^h(x,y) = s \left\{ \begin{array}{c} c_1 + c_2 x \\ c_3 + c_4 y \end{array} \right\} \tag{37}$$

on the sides of the square [13], originally denoted $BDFM_1$. In this case $\mathrm{div}\boldsymbol{p}^h = $ const. in Ω^e, as for RT_0. The normal trace is constant, as required, and the approximation can be specified by the four normal components of $\boldsymbol{p}^h$ on the boundary.

3.3 Neumann and Robin boundary conditions

So far, we have considered only the case of Dirichlet boundary conditions. Here, we propose a formulation of our method that preserves the structure of the element-level matrices (28) and (29) in the presence of Neumann and Robin boundary conditions as well. (Radiation boundary conditions that are employed to truncate unbounded domains are often expressed as Robin boundary conditions.)

Consider a partition of the domain boundary $\Gamma = \Gamma_D \cup \Gamma_R$, where $\Gamma_D \cap \Gamma_R = \emptyset$. We assume that the Dirichlet boundary condition on the entire domain boundary (2) is replaced by

11

$$u = g \qquad \text{on } \Gamma_{\mathrm{D}} \tag{38}$$

$$\mathcal{L}_{\mathrm{b}} u + \alpha u = \beta \qquad \text{on } \Gamma_{\mathrm{R}} \tag{39}$$

Here, $g{:}\,\Gamma_{\mathrm{D}} \to \mathbb{R}$, $\alpha{:}\,\Gamma_{\mathrm{R}} \to \mathbb{R}$, and $\beta{:}\,\Gamma_{\mathrm{R}} \to \mathbb{R}$ are given functions. Equation (39) represents a Robin boundary condition, as well as a Neumann condition in the special case $\alpha = 0$.

We extend $\boldsymbol{p}$ to Γ_{R} as follows

$$\mathcal{W} = \{\boldsymbol{p} \mid \boldsymbol{p} \in H\,(\mathrm{div};\Omega)\,,\ \boldsymbol{p} \cdot \boldsymbol{n} = -\beta \text{ on } \Gamma_{\mathrm{R}}\} \tag{40}$$

The functional (10) is modified

$$\Pi(u, \boldsymbol{p}) = \frac{1}{2}\,a(u, u) + \frac{1}{2}\,\langle \alpha u, u \rangle_{\Gamma_{\mathrm{R}}} - \langle \boldsymbol{p} \cdot \boldsymbol{n}, u \rangle_{\widetilde{\Gamma}} - L(u) - L_{\mathrm{b}}(\boldsymbol{p}) \tag{41}$$

This leads to the modified weak form

$$a(v, u) + \langle \alpha u, v \rangle_{\Gamma_{\mathrm{R}}} - \langle \boldsymbol{p} \cdot \boldsymbol{n}, v \rangle_{\widetilde{\Gamma}} = L(v) \tag{42}$$

$$- \langle \boldsymbol{q} \cdot \boldsymbol{n}, u \rangle_{\widetilde{\Gamma}} \qquad\qquad = L_{\mathrm{b}}(\boldsymbol{q}) \tag{43}$$

Here, $\boldsymbol{q} \in \mathcal{W}_0 = \{\boldsymbol{q} \mid \boldsymbol{q} \in H\,(\mathrm{div};\Omega)\,,\ \boldsymbol{q} \cdot \boldsymbol{n} = 0 \text{ on } \Gamma_{\mathrm{R}}\}$. The Euler-Lagrange equation (19) is now replaced by

$$\boldsymbol{p} \cdot \boldsymbol{n} = \mathcal{L}_{\mathrm{b}} u \qquad \text{on } \Gamma_{\mathrm{int}} \cup \Gamma_{\mathrm{D}} \tag{44}$$

$$\boldsymbol{p} \cdot \boldsymbol{n} = \mathcal{L}_{\mathrm{b}} u + \alpha u \quad \text{on } \Gamma_{\mathrm{R}} \tag{45}$$

For Neumann boundary conditions ($\alpha = 0$) the definition of $\boldsymbol{p}$ is unchanged.

The discretization of the above formulation retains the element-level matrices (28) and (29). The assembly process now has to account for the enforcement of the values of $\boldsymbol{p} \cdot \boldsymbol{n}$ on Γ_{R} as essential boundary conditions, in the same manner that Dirichlet boundary conditions are enforced in conventional finite element methods. In other words, the element-level degrees of freedom associated with $\boldsymbol{p} \cdot \boldsymbol{n}$ on Γ_{R} are not assembled into the global coefficient matrix. Instead, for inhomogeneous data ($\beta \neq 0$), they lead to the usual terms on the right-hand side. This discretization process is summarized in Table 2, which outlines the modification of Table 1 to account for Neumann and Robin boundary conditions.

Table 2
Correspondence between the global matrices in (27) and terms in the Galerkin equations, accounting for Neumann and Robin boundary conditions.

Matrix	Galerkin term
$\mathbf{K}^{\mathrm{PP}}$	$a(v^{\mathrm{P}}, u^{\mathrm{P}}) + \langle \alpha u^{\mathrm{P}}, v^{\mathrm{P}} \rangle_{\Gamma_{\mathrm{R}}}$
$\mathbf{K}^{\mathrm{PE}}$	$a(v^{\mathrm{P}}, u^{\mathrm{E}}) + \langle \alpha u^{\mathrm{E}}, v^{\mathrm{P}} \rangle_{\Gamma_{\mathrm{R}}}$
$\mathbf{K}^{\mathrm{PC}}$	$-\langle \boldsymbol{p}^h \cdot \boldsymbol{n}, v^{\mathrm{P}} \rangle_{\Gamma_{\mathrm{D}}}$
$\mathbf{K}^{\mathrm{EP}}$	$a(v^{\mathrm{E}}, u^{\mathrm{P}}) + \langle \alpha u^{\mathrm{P}}, v^{\mathrm{E}} \rangle_{\Gamma_{\mathrm{R}}}$
$\mathbf{K}^{\mathrm{EE}}$	$a(v^{\mathrm{E}}, u^{\mathrm{E}}) + \langle \alpha u^{\mathrm{E}}, v^{\mathrm{E}} \rangle_{\Gamma_{\mathrm{R}}}$
$\mathbf{K}^{\mathrm{EC}}$	$-\langle \boldsymbol{p}^h \cdot \boldsymbol{n}, v^{\mathrm{E}} \rangle_{\Gamma_{\mathrm{int}} \cup \Gamma_{\mathrm{D}}}$
$\mathbf{K}^{\mathrm{CP}}$	$-\langle \boldsymbol{q}^h \cdot \boldsymbol{n}, u^{\mathrm{P}} \rangle_{\Gamma_{\mathrm{D}}}$
$\mathbf{K}^{\mathrm{CE}}$	$-\langle \boldsymbol{q}^h \cdot \boldsymbol{n}, u^{\mathrm{E}} \rangle_{\Gamma_{\mathrm{int}} \cup \Gamma_{\mathrm{D}}}$
$\mathbf{F}^{\mathrm{P}}$	$L(v^{\mathrm{P}}) + \langle \beta, v^{\mathrm{P}} \rangle_{\Gamma_{\mathrm{R}}}$
$\mathbf{F}^{\mathrm{E}}$	$L(v^{\mathrm{E}}) + \langle \beta, v^{\mathrm{E}} \rangle_{\Gamma_{\mathrm{R}}}$
$\mathbf{F}^{\mathrm{C}}$	$L_{\mathrm{b}}(\boldsymbol{q}^h)$

3.4 Integration

Recall the selection of enrichment functions that are free-space homogeneous solutions, i.e., satisfying (21). This property leads to an alternate form of integration, namely

$$a(v, u^{\mathrm{E}}) = \langle \mathcal{L}_{\mathrm{b}} u^{\mathrm{E}}, v \rangle_{\widetilde{\Gamma}} \qquad (46)$$

cf. (11). Integration in element domains is replaced by integration along element boundaries. Similarly, integration of the constraint terms is performed along element boundaries rather than in element domains, see Eqn. (9).

The enrichment functions are chosen among solutions of the homogeneous form of the partial differential equation, which may vary rapidly. For this reason, integration of terms involving the enrichment functions may require more care than standard finite element polynomials. Various procedures for the integration of oscillatory functions, e.g., [20, 11, 23], may be employed for this purpose.

4 Application to the Helmholtz Equation

The Helmholtz operator, describing time-harmonic acoustic and electromagnetic waves, may lose ellipticity with increasing wave number, since in that case the bilinear form no longer induces a norm. This is related to the pollution effect, in which finite element solutions of the Helmholtz equation differ significantly from the best approximation [4, 6, 12, 38], due to spurious dispersion in the computation. In practical terms, this leads to an increase in the cost of the finite element solution of the Helmholtz equation at higher wave numbers.

The Helmholtz equation is governed by the indefinite operator $\mathcal{L}u = -\Delta u - k^2 u$, with given wave number k. The weak operator in this case is $a(v, u) = (\nabla v, \nabla u)_{\widetilde{\Omega}} - (v, k^2 u)$. The corresponding boundary operator is the normal derivative, namely $\mathcal{L}_{\mathrm{b}} u = \boldsymbol{n} \cdot \nabla u$. A natural choice for the scaling factor is $s = k$.

Element-level basis functions for u^{E} that satisfy (21) for constant k are plane waves of the form $\exp(\mathrm{i}\, \boldsymbol{k} \cdot \boldsymbol{x})$, where $|\boldsymbol{k}| = k$. For a plane wave propagating in the θ-direction in two dimensions, $\boldsymbol{k}^T = k\,[\cos\theta, \sin\theta]$. Since the dominant directions of propagation cannot generally be anticipated, a likely implementation of DEM for acoustics is based on an enrichment that is spanned by an even number of plane waves such that for every wave going in one direction there is another one going in the opposite direction. In this case, the complex exponential representations of plane waves can be replaced by *real*-valued trigonometric basis functions. Use of such functions simplifies the formation of the matrices associated with the enrichment. An additional consequence of this alternative representation is that in this case, a conjugated formulation with sesquilinear operators is equivalent to a non-conjugated formulation with bilinear operators.

Finally, we note that regularization of the enrichment could be needed to circumvent potential element-level resonance at resolutions below two points per wavelength. If needed, a procedure proposed in [28] for regularizing subdomains can be incorporated in the DEM formulation to regularize elements and thereby overcome this difficulty.

4.1 One dimension: P_1-2-P_1

Here, we consider standard two-noded linear interpolation (P_1) of u^{P}, and enrichment that is spanned by *two* plane waves propagating in the positive and negative axis directions. The Lagrange multipliers are also linear in the element with nodal values that enforce inter-element continuity.

4.1.1 Dispersion analysis

We consider a uniform mesh of elements of size h with nodes at $x_A = Ah$, $A \in \mathbb{Z}$. The two fields of the statically condensed u^{P}-$\boldsymbol{p}$ formulation decouple in this case, simplifying the analysis.

We start with the polynomial field. Consider an exact solution representing an outgoing plane wave with nodal values given by

$$u(x_A) = (\exp(\mathrm{i}\,kh))^A \tag{47}$$

We assume corresponding nodal values of the finite element polynomial field of the form

$$u_A^{\mathrm{P}} = \left(\exp\left(\mathrm{i}\,k^{\mathrm{P}}h\right)\right)^A \tag{48}$$

where $u_A^{\mathrm{P}} = u^{\mathrm{P}}(x_A)$. The dependence of the approximate wave number of the polynomial field, k^{P}, on wave resolution ($G = 2\pi/(kh)$ points per wavelength) is determined by the analysis of a standard three-node stencil.

The P_1-2-P_1 DEM element yields the following equation for the uncoupled u^{P} field at interior node A

$$-\left(\left(1 + (kh)^2/6\right)\sin(kh) - kh\right)u_{A-1}^{\mathrm{P}} + 2\left(\left(1 - (kh)^2/3\right)\sin(kh) - kh\cos(kh)\right)u_A^{\mathrm{P}} -$$
$$\left(\left(1 + (kh)^2/6\right)\sin(kh) - kh\right)u_{A+1}^{\mathrm{P}} = 0 \quad (49)$$

Substituting (48) leads to

$$0 = -\left(\left(1 + (kh)^2/6\right)\sin(kh) - kh\right)\Big/\exp\left(\mathrm{i}\,k^{\mathrm{P}}h\right) + \tag{50}$$
$$2\left(\left(1 - (kh)^2/3\right)\sin(kh) - kh\cos(kh)\right) - \left(\left(1 + (kh)^2/6\right)\sin(kh) - kh\right)\exp\left(\mathrm{i}\,k^{\mathrm{P}}h\right)$$
$$= -2\left(\left(1 + (kh)^2/6\right)\sin(kh) - kh\right)\cos\left(k^{\mathrm{P}}h\right) + \tag{51}$$
$$2\left(\left(1 - (kh)^2/3\right)\sin(kh) - kh\cos(kh)\right)$$

Thus, the plane wave dispersion relation for the polynomial field is

$$\cos\left(k^{\mathrm{P}}h\right) = \frac{kh\cos(kh) - (1 - (kh)^2/3)\sin(kh)}{kh - (1 + (kh)^2/6)\sin(kh)} \tag{52}$$

The approximate wave number k^{P} is purely imaginary for resolutions over two points per wavelength since

$$\cos\left(k^{\mathrm{P}}h\right) < -1, \qquad kh < \pi \tag{53}$$

15
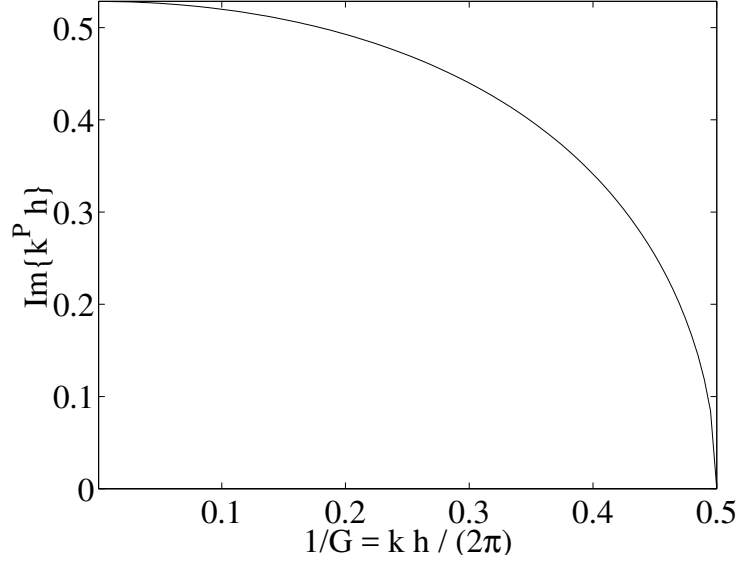
Fig. 2. Damping in polynomial field in one dimension.

indicating strong damping of the polynomial field. Figure 2 shows the variation of the imaginary part of k^{P} with wave resolution. In the limit of high resolution, we have

$$\lim_{kh \to 0} \cos\left(k^{\mathrm{P}} h\right) = -\frac{8}{7} \tag{54}$$

which corresponds to a damping factor of 0.59.

The Lagrange multipliers are related to normal derivatives. Nodal values of the derivative of an exact solution representing an outgoing plane wave are given by

$$u_{,x}(x_A) = \mathrm{i}\, k \left(\exp(\mathrm{i}\, kh)\right)^A \tag{55}$$

We assume corresponding nodal values of the finite element constraint field in the form

$$\boldsymbol{p}_A = \mathrm{i}\, k \left(\exp\left(\mathrm{i}\, k^{\mathrm{C}} h\right)\right)^A \tag{56}$$

where $\boldsymbol{p}_A = \boldsymbol{p}^h(x_A)$. Recall, $\boldsymbol{p}$ is defined as a d-dimensional vector, so that in this case it is a scalar. The dependence of the approximate wave number of the constraint field, k^{C}, on wave resolution is again determined by the analysis of a standard three-node stencil.

The P_1-2-P_1 DEM element yields the following equation for the uncoupled $\boldsymbol{p}$

16

field at interior node A

$$-\boldsymbol{p}_{A-1} + 2\cos(kh)\boldsymbol{p}_A - \boldsymbol{p}_{A+1} = 0 \tag{57}$$

Substituting (56) leads to

$$0 = -1 \Big/ \exp\left(\mathrm{i}\,k^{\mathrm{C}}h\right) + 2\cos(kh) - \exp\left(\mathrm{i}\,k^{\mathrm{C}}h\right) \tag{58}$$

$$= -2\cos\left(k^{\mathrm{C}}h\right) + 2\cos(kh) \tag{59}$$

Thus, the Lagrange multipliers are *free of dispersion* in one dimension.

In one-dimensional Dirichlet problems with homogeneous equations (i.e., $f = 0$), the polynomial field vanishes completely. In this case, the enrichment u^{E}, and hence the resulting total field u^h, is exact (and continuous).

4.1.2 Numerical results

We consider a problem in an interval of length a for the homogeneous Helmholtz equation ($f = 0$). Dirichlet boundary conditions, $u(0) = 1$ and $u(a) = \exp(\mathrm{i}ka)$, are specified so that the exact solution is

$$u = \exp(\mathrm{i}kx) \tag{60}$$

The interval is discretized by a uniform mesh of the P_1-2-P_1 elements described in the beginning of this section. A series of tests was performed for $ka = 10$ and 30, with resolutions down to 0.42 points per wavelength. As expected, in all the tests performed, u^{P} was zero and u^{E} was exact, to the limit of machine precision.

Figures 3 and 4 show examples of solutions, obtained at a resolution of 6.28 points per wavelength, for $ka = 10$ and 30, respectively. Results obtained by the Galerkin method are shown for comparison. Spurious dispersion of the Galerkin method is evident in both cases. The degradation at $ka = 30$ is a manifestation of pollution.

We now consider an inhomogeneous problem in order to highlight the role of the polynomial field. In this case $f = -2 - (kx)^2$, and Dirichlet boundary conditions, $u(0) = 1$ and $u(a) = 1 + \exp(\mathrm{i}ka)$, are specified. The exact solution

$$u = x^2 + \exp(\mathrm{i}kx) \tag{61}$$

is not contained in the finite element space. As before, a series of tests was performed for $ka = 10$ and 30, with resolutions down to 0.42 points per
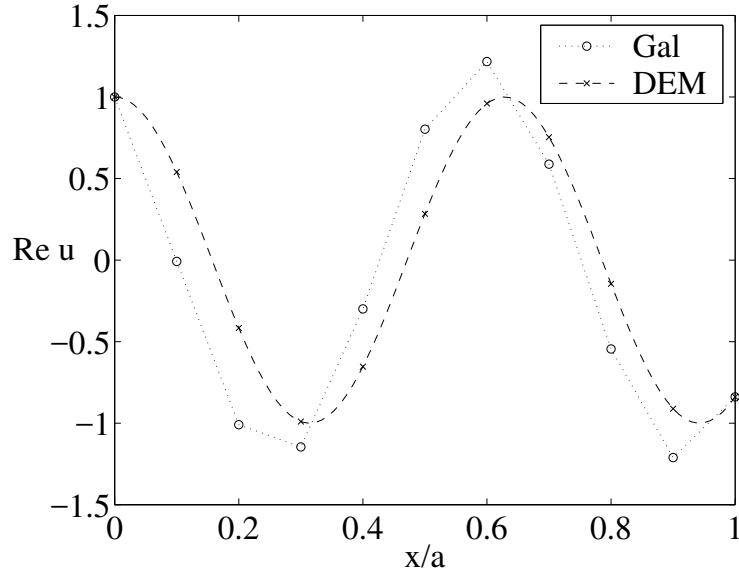
Fig. 3. Homogeneous problem in one dimension, $ka = 10$, 6.28 points per wavelength.
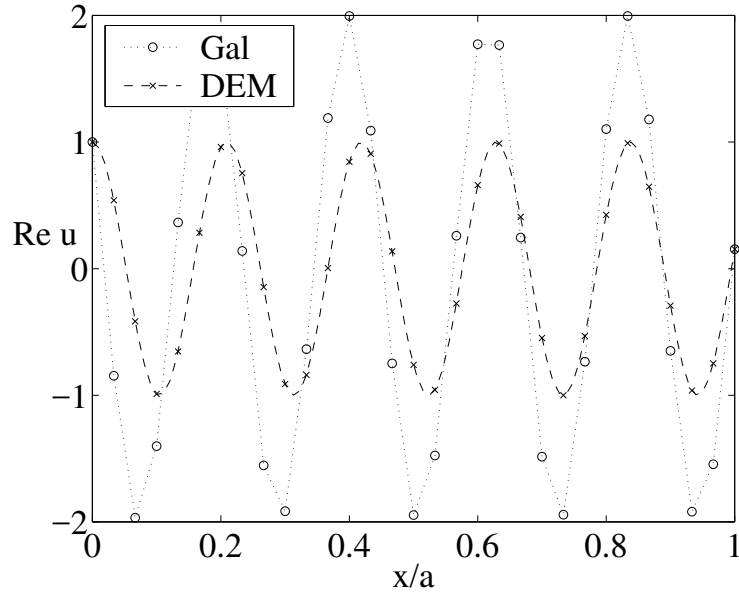
Fig. 4. Homogeneous problem in one dimension, $ka = 30$, 6.28 points per wavelength.

wavelength. It is remarkable that in all the tests performed, the DEM solution was continuous and nodally exact, to the order of machine precision.

Figure 5 shows an example of a solution to the inhomogeneous problem for $ka = 10$, at a low resolution of 3.77 points per wavelength. The DEM solution is virtually indistinguishable from the exact solution in the entire interval. The particular solution is shown in Fig. 6. The polynomial field u^{P} provides a good approximation of the piecewise linear nodal interpolant of the particular part of the exact solution.
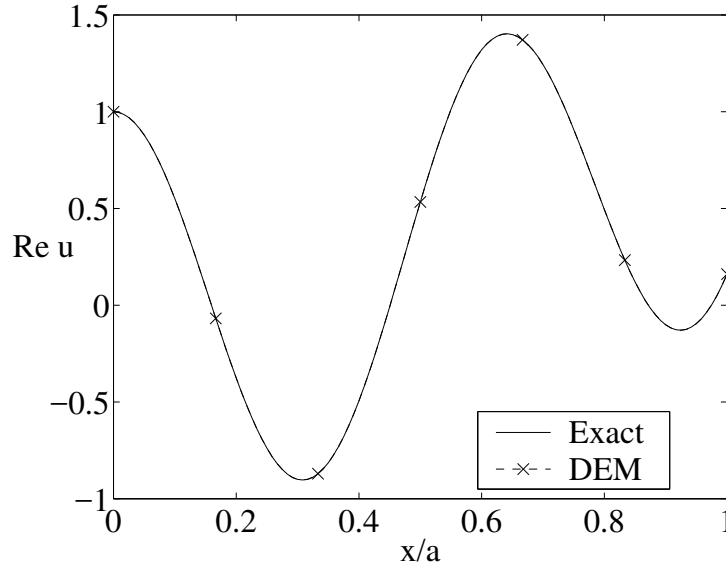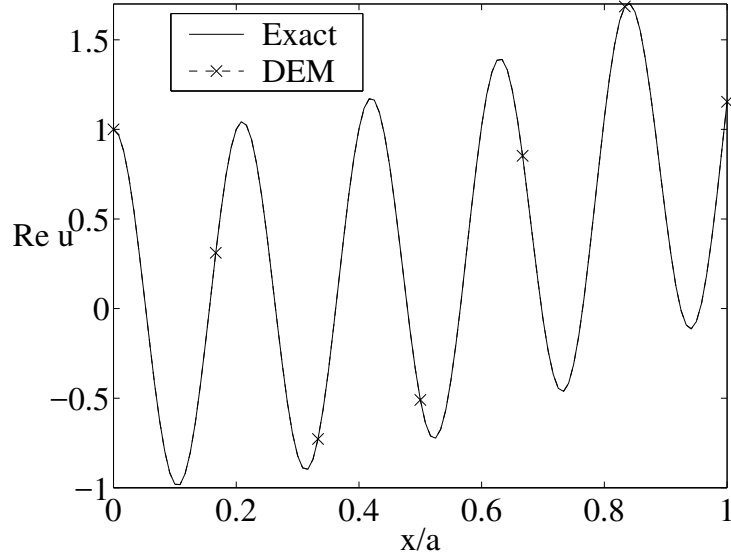
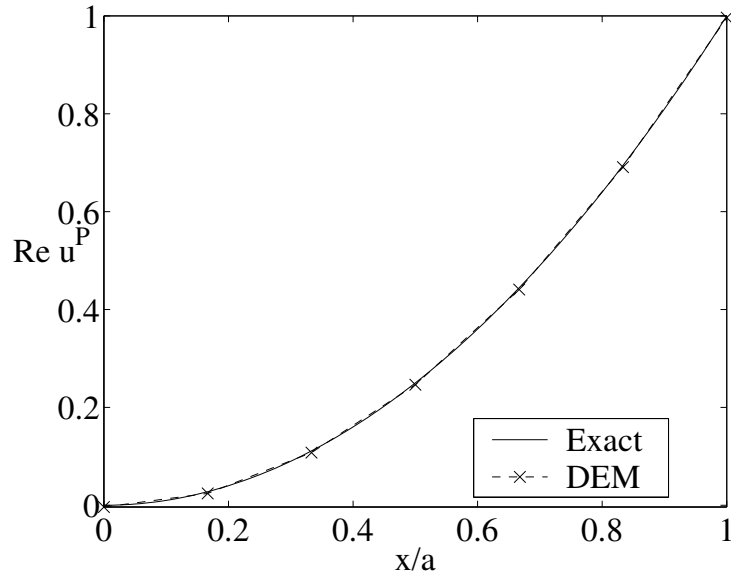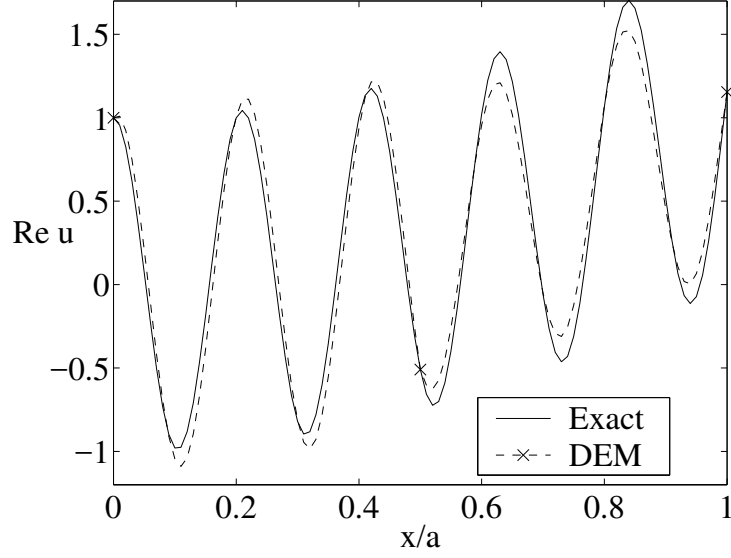Fig. 5. Inhomogeneous problem in one dimension, $ka = 10$, 3.77 points per wavelength.
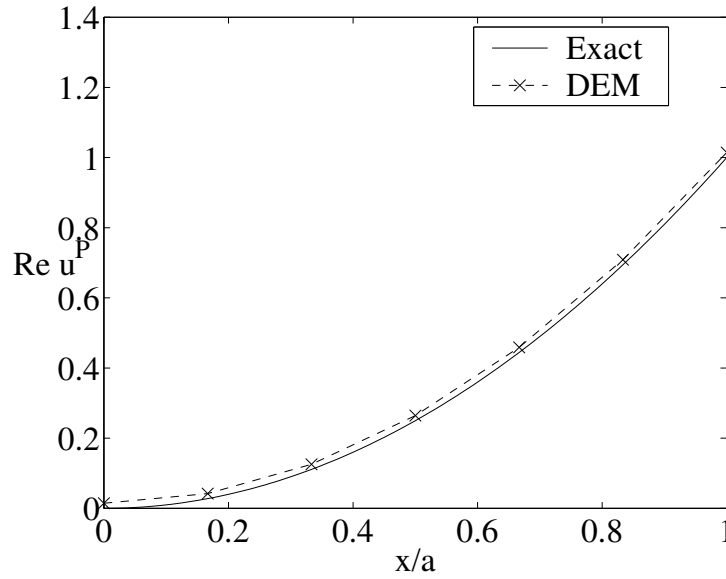
Fig. 6. Particular solution of inhomogeneous problem and u^P in one dimension, $ka = 10$, 3.77 points per wavelength.

These features of the DEM solution are retained when we reduce the resolution to a very low value of 1.26 points per wavelength (still at $ka = 10$, Figs. 7 and 8).

We now increase the wave number, $ka = 30$, keeping the resolution at the same value (1.26 points per wavelength). The DEM solution provides an excellent representation of the exact solution in the entire domain (Fig. 9). The particular solution is shown in Fig. 10. The polynomial field u^P provides an
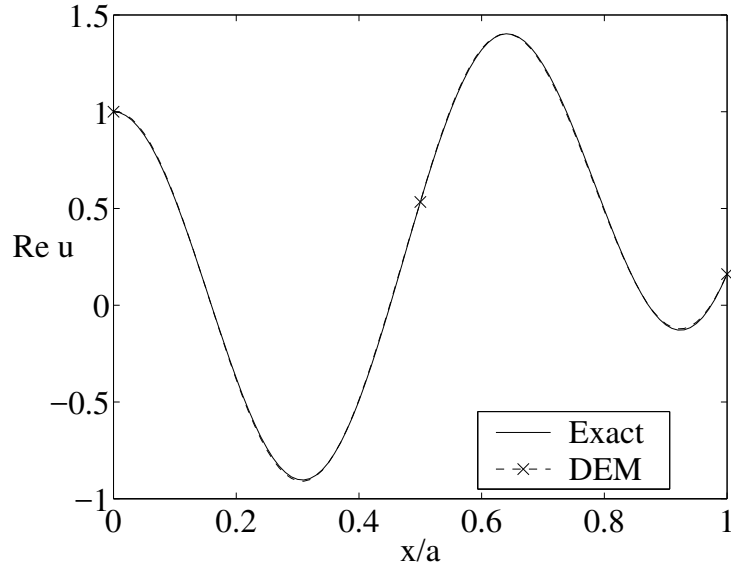
Fig. 7. Inhomogeneous problem in one dimension, $ka = 10$, 1.26 points per wavelength.
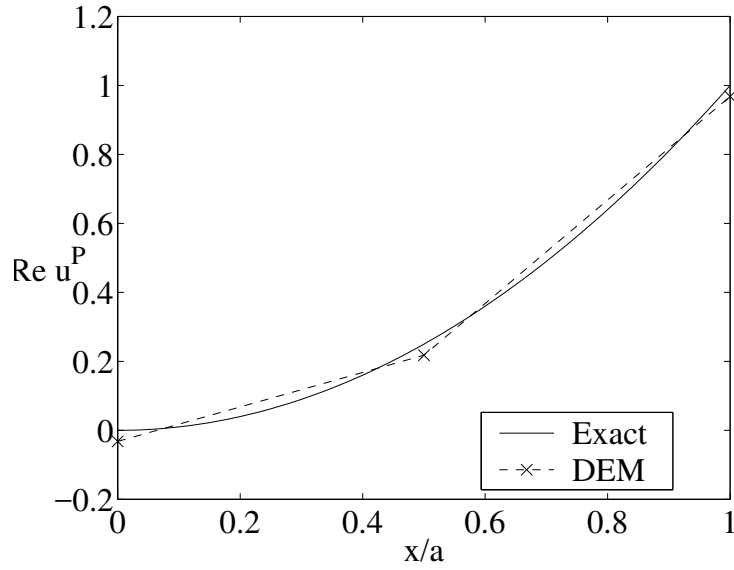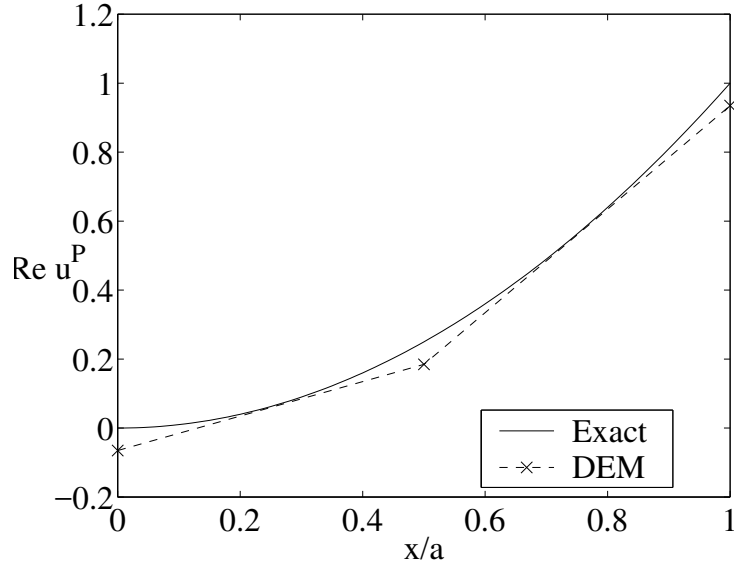

Fig. 8. Particular solution of inhomogeneous problem and u^P in one dimension, $ka = 10$, 1.26 points per wavelength.

excellent approximation of the the particular part of the exact solution.

The resolution is reduced further to an extremely low value of 0.42 points per wavelength (still at $ka = 30$, Figs. 11 and 12). The DEM solution retains nodal exactness, and although now distinguishable from the exact solution inside the elements, still provides a good approximation of the exact solution in the entire interval, considering the resolution.

Fig. 9. Inhomogeneous problem in one dimension, $ka = 30$, 1.26 points per wavelength.

Fig. 10. Particular solution of inhomogeneous problem and u^{P} in one dimension, $ka = 30$, 1.26 points per wavelength.

To summarize the DEM results of the inhomogeneous problem, we observe continuity and nodal exactness, to the order of machine precision, in all cases. In most of the computations the DEM solution is virtually indistinguishable from the exact solution in the entire interval. This property diminishes only at the extremely low resolution of 0.42 points per wavelength.

21

Fig. 11. Inhomogeneous problem in one dimension, $ka = 30$, 0.42 points per wavelength.

Fig. 12. Particular solution of inhomogeneous problem and u^P in one dimension, $ka = 30$, 0.42 points per wavelength.

4.2 Q_1-4-$BDFM_1$ quadrilateral

Next, we consider quadrilaterals with standard four-noded bilinear interpolation (Q_1) of u^P, represented schematically in Fig. 13. The enrichment is spanned by *four* plane waves propagating in the positive and negative axis directions. We employ the $BDFM_1$ approximation of Lagrange multipliers that are *constant* along the sides of the element (37).

22
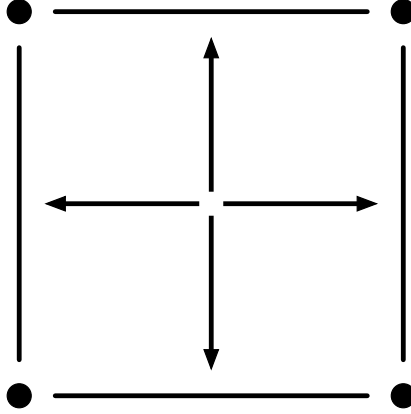
Fig. 13. Schematic of the Q_1-4-$BDFM_1$ quadrilateral.

The above choice of directions of propagation for the enrichment is motivated by the known performance of the standard Galerkin method with continuous piecewise polynomials [39]. The standard method performs best on structured meshes when element diagonals are aligned with directions of propagation. The worst performance is in the case of propagation along element sides.

4.2.1 Dispersion analysis

In two dimensions, we consider a uniform mesh of elements of size h, aligned with the global axes, with vertices at $\boldsymbol{x}_A = (mh, nh)$, $m, n \in \mathbb{Z}$. The two fields of the statically condensed u^P-$\boldsymbol{p}$ formulation again decouple in this case, simplifying the analysis.

The nodal points of the bilinear polynomial interpolation of u^P are at the vertices of the mesh $\boldsymbol{x}_A$. Consider an exact solution of the Helmholtz equation, representing a plane wave oriented at an angle θ to the mesh (not to be confused with the angles of the plane wave enrichment, which in this case are 0, $\pi/2$, π, and $3\pi/2$). Values of the exact solution at the nodal points are

$$u(\boldsymbol{x}_A) = (\exp(\mathrm{i}\, khc))^m (\exp(\mathrm{i}\, khs))^n \tag{62}$$

Here, $c = \cos\theta$ and $s = \sin\theta$. The dependence of the approximate wave number of the polynomial field, k^P, on the orientation and wave resolution is determined by the analysis of a standard nine-node patch (Fig. 14). The dispersion analysis reveals that, as in one dimension, there is strong damping of the polynomial field.

The dispersion analysis of the constraint field, which is related to normal derivatives, is less conventional. The connectivity of the piecewise-constant edge constraints leads to a seven-edge stencil in either the x- or y-directions (e.g., Fig. 15). We associate edge values of the piecewise constant constraints
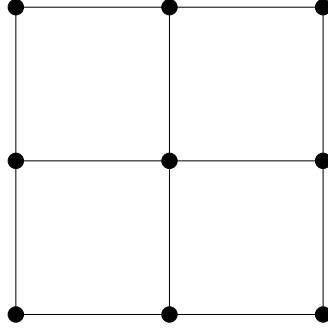
Fig. 14. A nine-node patch.

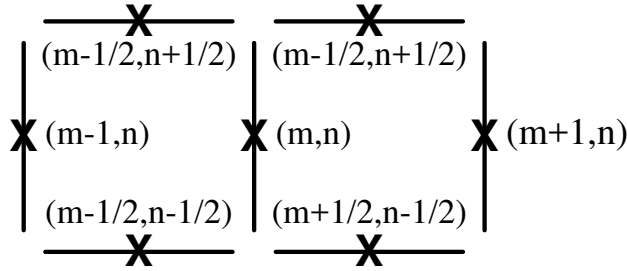

Fig. 15. A seven-edge stencil, centered around a degree of freedom that corresponds to the derivative with respect to x. The piecewise constant edge values are associated with the middle of each edge.

with the middle of each edge, with coordinates $\boldsymbol{x}_A = (mh, nh)$. The gradient of the exact solution is $iu\,\boldsymbol{k}$. Consequently, we assume edge values of the constraint field to be in the form

$$\boldsymbol{p}_A \cdot \boldsymbol{n} = \mathrm{i}\left(\exp(\mathrm{i}\,k^{\mathrm{C}}hc)\right)^m \left(\exp(\mathrm{i}\,k^{\mathrm{C}}hs)\right)^n \boldsymbol{k} \cdot \boldsymbol{n} \tag{63}$$

Here, $\boldsymbol{p}_A = \boldsymbol{p}^h(\boldsymbol{x}_A)$ and $\boldsymbol{n}$ is the outward unit vector normal to the element boundary.

The dependence of the approximate wave number of the constraint field, k^{C}, on the orientation and wave resolution is determined by the analysis of a combination of four seven-edge stencils, two in the x-direction and two in the y-direction (Fig. 16).

This yields the following plane wave dispersion relation for the constraint field

$$
\begin{aligned}
c\,\Big(kh\left(\cos(kh) - \cos\left(k^{\mathrm{C}}hc\right)\right)\cos\left(k^{\mathrm{C}}hs/2\right) + \\
\sin(kh)\sin\left(k^{\mathrm{C}}hc\right)\sin\left(k^{\mathrm{C}}hs/2\right)\Big) + \\
s\,\Big(kh\left(\cos(kh) - \cos\left(k^{\mathrm{C}}hs\right)\right)\cos\left(k^{\mathrm{C}}hc/2\right) + \\
\sin(kh)\sin\left(k^{\mathrm{C}}hs\right)\sin\left(k^{\mathrm{C}}hc/2\right)\Big) = 0
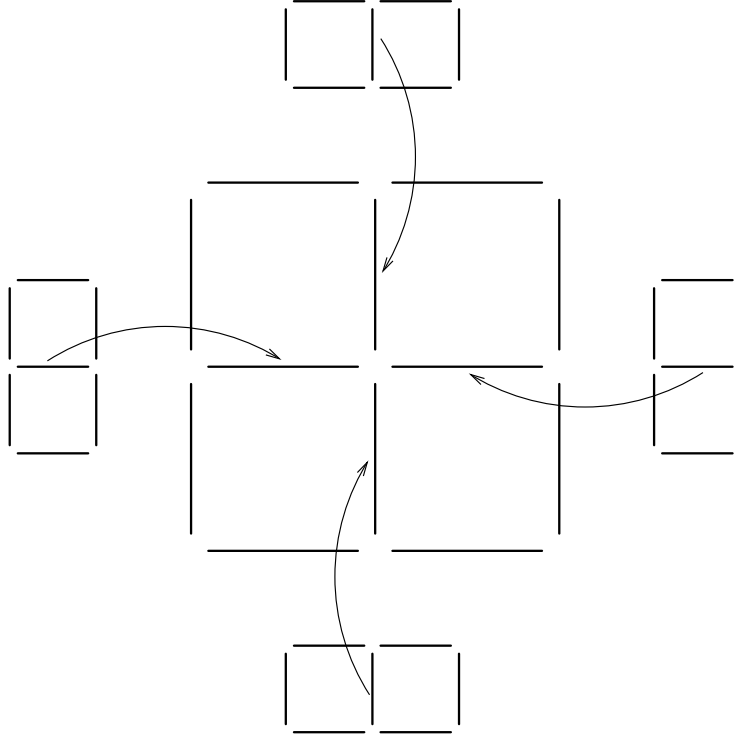\end{aligned}
\tag{64}
$$

24

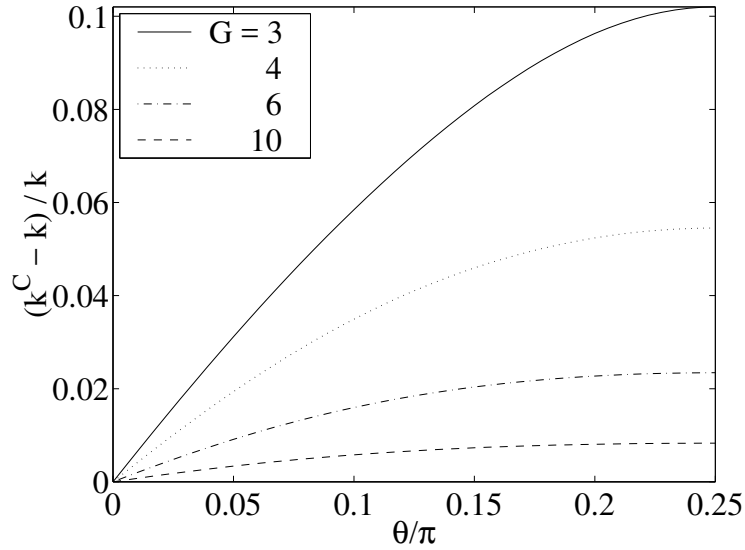Fig. 16. A twelve-edge stencil composed of four seven-edge stencils.

Fig. 17. Dispersion in constraint field at various resolutions, $G = 2\pi/(kh)$.

The constraint field exhibits excellent dispersion properties at angles up to 10° from the direction of any of the four plane waves in the enrichment at all resolutions (Fig. 17). At larger angles, there is a deterioration at very low resolutions ($G < 4$ points per wavelength).
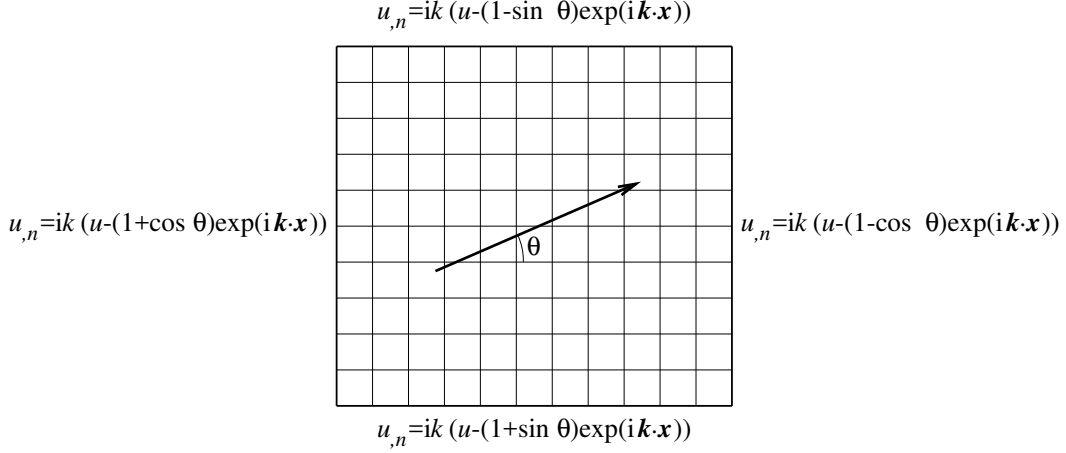
$u_{,n} = \mathrm{i}k\,(u - (1 - \sin\,\theta)\exp(\mathrm{i}\boldsymbol{k}\!\cdot\!\boldsymbol{x}))$

$u_{,n} = \mathrm{i}k\,(u - (1 + \cos\,\theta)\exp(\mathrm{i}\boldsymbol{k}\!\cdot\!\boldsymbol{x}))$
θ
$u_{,n} = \mathrm{i}k\,(u - (1 - \cos\,\theta)\exp(\mathrm{i}\boldsymbol{k}\!\cdot\!\boldsymbol{x}))$

$u_{,n} = \mathrm{i}k\,(u - (1 + \sin\,\theta)\exp(\mathrm{i}\boldsymbol{k}\!\cdot\!\boldsymbol{x}))$

Fig. 18. Problem statement.

4.2.2 Numerical results

The favorable dispersion results outlined above are supported by accurate solutions that are obtained by several numerical tests. In the following, we report on some of these tests, and compare the conditioning of the proposed discretization method with that of PUM.

We consider a problem in an $a \times a$ square, discretized by a uniform 10×10 mesh composed of the Q_1-4-$BDFM_1$ elements described in the beginning of this section (Fig. 18). Inhomogeneous Robin boundary conditions are specified so that the exact solution is a plane wave propagating in a given direction.

The error for a plane wave oriented almost along the x-axis ($\theta = 0.01°$) is shown in Fig. 19. In this case, one of the angles of the enrichment practically coincides with the direction of the solution, and the error of DEM is four orders of magnitude smaller than that of the standard Galerkin method. The enriched method retains its superior performance, albeit to a lesser degree, even when the direction of the solution differs significantly from all of the angles of the enrichment (at an angle of 77°, see Fig. 20). The error in the enriched method is now a factor of two to four smaller than the Galerkin method. Clearly, the situation for DEM will improve when the enrichment is refined by adding plane wave directions. It is striking that in both cases the enriched method seems to exhibit no pollution (the error appears to depend only on resolution, not ka), in contrast to the Galerkin method. This feature may stem from the lack of accumulation of dispersion due to the discontinuous nature of the DEM approximation.

The conditioning of the coefficient matrices is presented in Fig. 21 (for a plane wave at 77° and $ka = 20$). The Q_1-4-$BDFM_1$ DEM element is in the condensed u^{P}-$\boldsymbol{p}$ form with diagonal scaling to account for the different orders of the two fields. The improvement of DEM over PUM (with four plane waves

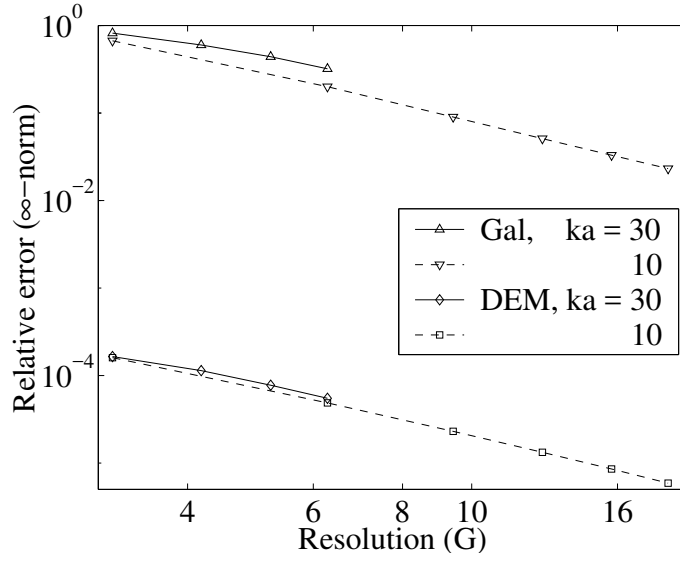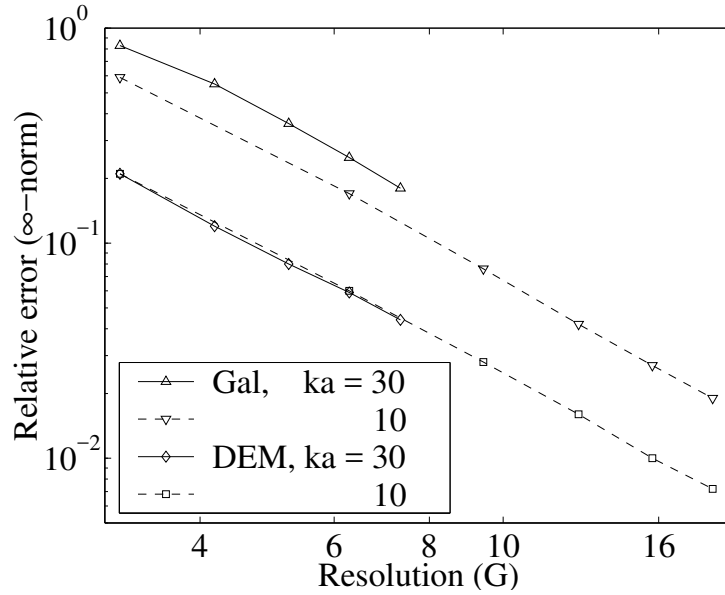Fig. 19. Relative error for a plane wave at $0.01°$.

Fig. 20. Relative error for a plane wave at $77°$.

in the enrichment) is evident, a factor of over 10^4 at a resolution of 10, with a distinctly lower increase rate. There is a degradation in the conditioning of the enriched method compared to the Galerkin method at a given resolution, which is expected. Yet, this degradation is not prohibitive in absolute terms. As a matter of fact, the conditioning of the enriched method appears to be of the same order as that of the Galerkin method *for a given accuracy.*

27
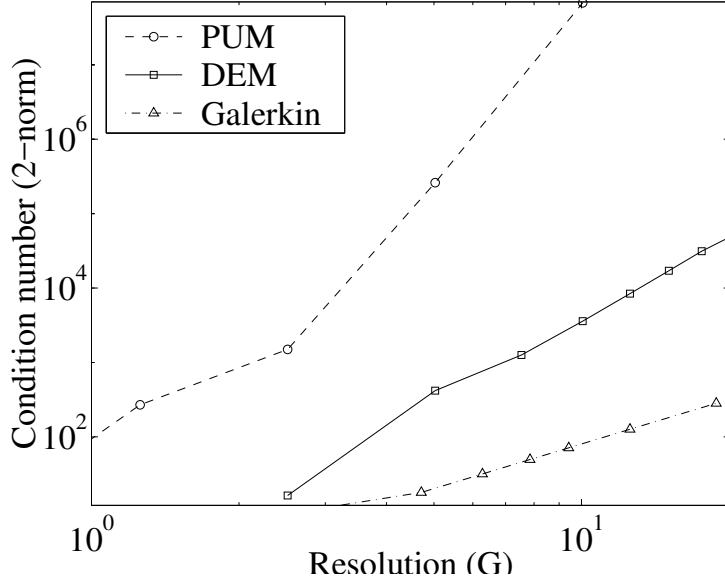
Fig. 21. Condition number at $ka = 20$ and $\theta = 77°$.

4.2.3 Computational cost

We briefly comment on the relative cost of using $Q_1\text{-}4\text{-}BDFM_1$ DEM elements, by simply counting the number of degrees of freedom employed on a given mesh. We consider a problem in a square domain, discretized by a uniform mesh of $n \times n$ elements. Such a mesh has $(n+1)^2$ vertices and $2n(n+1)$ edges.

Solving this problem with Q_1 Galerkin elements employs $(n+1)^2$ vertex degrees of freedom. The statically condensed $Q_1\text{-}4\text{-}BDFM_1$ DEM elements require $(n+1)^2$ vertex degrees of freedom and $2n(n+1)$ edge degrees of freedom. This observation is essentially independent of the local dimension (i.e., the number of plane wave directions) of the enrichment. Thus, for $n \gg 1$, there are three times more DEM degrees of freedom than Galerkin. PUM has nodal degrees of freedom, but there are $\dim u^{\mathrm{E}}$ degrees of freedom per node (with the added effect of degrading sparseness). Thus, there are $\dim u^{\mathrm{E}}$ times more PUM degrees of freedom than Galerkin. For example, the numerical tests in [47] employ 18 to 36 plane wave directions. In such cases, there are six to 12 times more PUM degrees of freedom than DEM!

5 Application to Advection-diffusion

Advection-diffusion describes many transport phenomena and serves as a model for fluid mechanics. The computation of convection-dominated transport phenomena by standard methods is fraught with difficulties, primarily spurious oscillations.

28

The advection-diffusion equation is governed by the nonsymmetric operator $\mathcal{L}u = -\nabla \cdot (\kappa \nabla u) + \boldsymbol{a} \cdot \nabla u$, with given diffusivity $\kappa > 0$ and flow velocity $\boldsymbol{a}$. The bilinear operator in this case is $a(v, u) = (\nabla v, \kappa \nabla u)_{\widetilde{\Omega}} + (v, \boldsymbol{a} \cdot \nabla u)$. The corresponding boundary operator is the flux, namely $\mathcal{L}_{\mathrm{b}}u = \kappa \boldsymbol{n} \cdot \nabla u$. A natural choice for the scaling factor is $s = |\boldsymbol{a}|$. The numerical formulation cannot be derived from the Lagrangian (10), but nonetheless it is based on the weak form (14) and (15).

Element-level basis functions for u^{E} that satisfy (21) are a constant and, for constant coefficients, $\exp(\boldsymbol{a} \cdot \boldsymbol{x}/\kappa)$. Since the constant is already contained in the underlying polynomial space, a likely implementation of DEM for advection-diffusion is based on an enrichment that is spanned by the single exponential basis function in each element.

Let u^{E} be spanned by a single enrichment basis function N_e^{E} in each element

$$u^{\mathrm{E}}(\boldsymbol{x}) = \sum_{e=1}^{n_{\mathrm{el}}} u_e^{\mathrm{E}} N_e^{\mathrm{E}}(\boldsymbol{x}), \quad \boldsymbol{x} \in \Omega^e \tag{65}$$

The enrichment basis function in each element should be scaled to preclude excessively high numerical values in convection-dominated regimes. This is accomplished by simply employing

$$N_e^{\mathrm{E}} = \exp\left(\boldsymbol{a} \cdot (\boldsymbol{x} - \boldsymbol{x}_0^e)/\kappa\right) \tag{66}$$

Here, $\boldsymbol{x}_0^e \in \Gamma^e$ is a reference point that is chosen to satisfy $\boldsymbol{a} \cdot \boldsymbol{x}_0^e \geq \boldsymbol{a} \cdot \boldsymbol{x}$, $\forall \boldsymbol{x} \in \Omega^e$, so that $0 < N_e^{\mathrm{E}} \leq 1$.

5.1 Static condensation

Substituting Eqn. (65), and $v^{\mathrm{E}} = N_e^{\mathrm{E}}$ in Ω^e and zero elsewhere into Eqn. (25) provides the element-level equation

$$a(N_e^{\mathrm{E}}, u^{\mathrm{P}})_{\Omega^e} + u_e^{\mathrm{E}} a(N_e^{\mathrm{E}}, N_e^{\mathrm{E}})_{\Omega^e} + \left\langle \boldsymbol{p}^h \cdot \boldsymbol{n}, N_e^{\mathrm{E}} \right\rangle_{\Gamma^e} = L^e(N_e^{\mathrm{E}}) \tag{67}$$

where all operators are restricted to element e. Thus

$$u_e^{\mathrm{E}} = \frac{L^e(N_e^{\mathrm{E}}) - a(N_e^{\mathrm{E}}, u^{\mathrm{P}})_{\Omega^e} - \left\langle \boldsymbol{p}^h \cdot \boldsymbol{n}, N_e^{\mathrm{E}} \right\rangle_{\Gamma^e}}{\langle \kappa \boldsymbol{n} \cdot \nabla N_e^{\mathrm{E}}, N_e^{\mathrm{E}} \rangle_{\Gamma^e}}, \qquad e = 1, \ldots, n_{\mathrm{el}} \tag{68}$$

exploiting the fact that $\mathcal{L}N_e^{\mathrm{E}} = 0$. (Note that for N_e^{E} defined in (66), $\langle \kappa \boldsymbol{n} \cdot \nabla N_e^{\mathrm{E}}, N_e^{\mathrm{E}} \rangle_{\Gamma^e} = \left(\boldsymbol{a} \cdot \boldsymbol{n}, N_e^{\mathrm{E}^2}\right)_{\Gamma^e}$.) The above expression provides a representa-
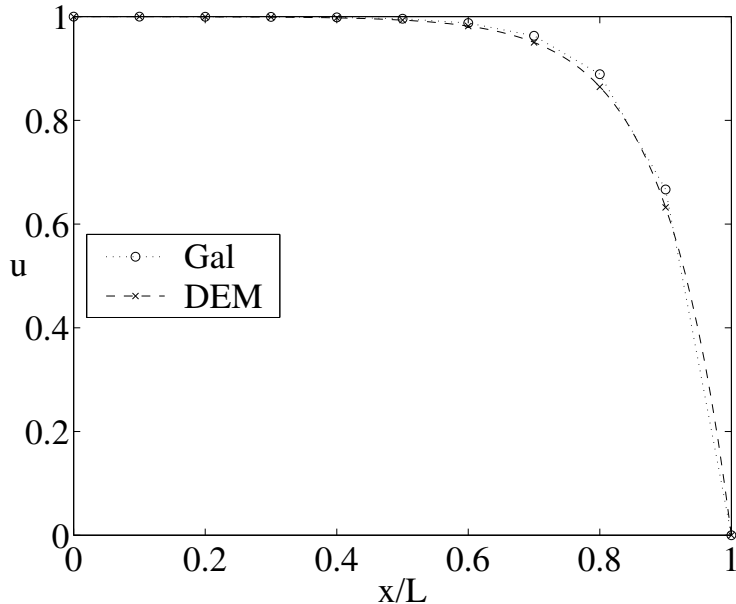
Fig. 22. Homogeneous problem in one dimension, $\alpha = 0.5$.

tion of u^{E} in the element in terms of the loading, and u^{P} and $\boldsymbol{p}^h$ restricted to the element. Employing this expression in (65) and substituting into (24) and (26) leads to a u^{P}-$\boldsymbol{p}$ formulation that does not require inversion of a matrix operator.

5.2   Numerical results

We consider a one-dimensional problem in an interval of length L for the homogeneous advection-diffusion equation $(f = 0)$. Dirichlet boundary conditions, $u(0) = 1$ and $u(L) = 0$, are specified so that the exact solution is

$$u = \frac{\exp(a(x - L)/\kappa) - 1}{\exp(-aL/\kappa) - 1} \tag{69}$$

The interval is discretized by a uniform mesh of 10 P_1-1-P_1 DEM elements. A series of tests was performed with element Péclet numbers, $\alpha = \dfrac{ah}{2\kappa}$, up to 10^6. As expected, in all the tests performed, the DEM solution is continuous and exact to the limit of machine precision.

Figures 22 and 23 show examples of solutions, obtained at $\alpha = 0.5$ and 5, respectively. Results obtained by the Galerkin method are shown for comparison. There is an error in the Galerkin solution even at a relatively low value of $\alpha = 0.5$ (Fig. 22), before the onset of spurious oscillations at $\alpha = 1$. Spurious oscillations pollute the Galerkin solution at $\alpha = 5$ (Fig. 23).
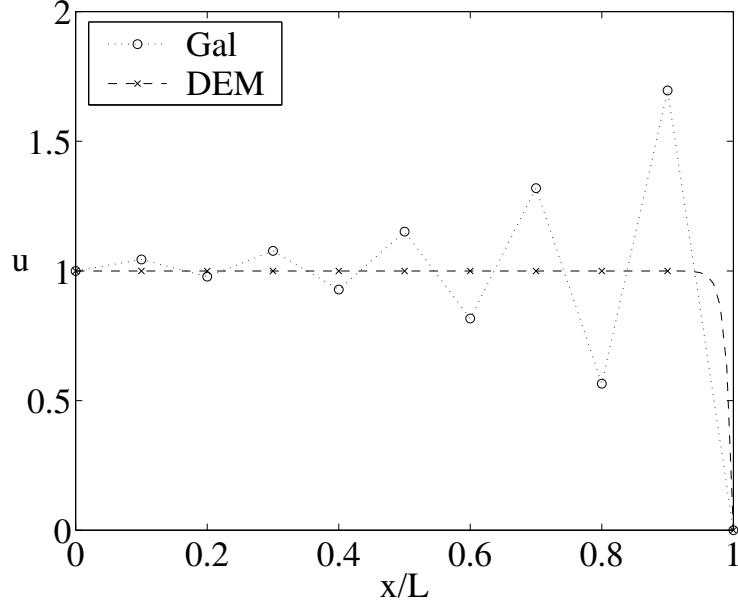
Fig. 23. Homogeneous problem in one dimension, $\alpha = 5$.

We now consider an inhomogeneous problem in order to highlight the role of the polynomial field. In this case $f = 2(ax - \kappa)$ with homogenous Dirichlet boundary conditions. The exact solution

$$u = \left(\frac{x}{L}\right)^2 - \frac{\exp(a(x - L)/\kappa) - \exp(-aL/\kappa)}{1 - \exp(-aL/\kappa)} \tag{70}$$

is not contained in the finite element space. As before, a series of tests was performed with element Péclet numbers up to 10^6.

Figure 24 shows an example of a solution to the inhomogeneous problem at a low value of $\alpha = 1$. The DEM solution is virtually indistinguishable from the exact solution in the entire interval. The particular solution is shown in Fig. 25. The polynomial field u^{P} provides an excellent approximation of the piecewise linear nodal interpolant of the particular part of the exact solution.

We now consider the advection dominated case with $\alpha = 10^6$. The DEM solution provides an excellent representation of the exact solution in the entire domain (Fig. 26), including the thin boundary layer. The particular solution is shown in Fig. 27. The polynomial field u^{P} provides an excellent approximation of the the particular part of the exact solution.
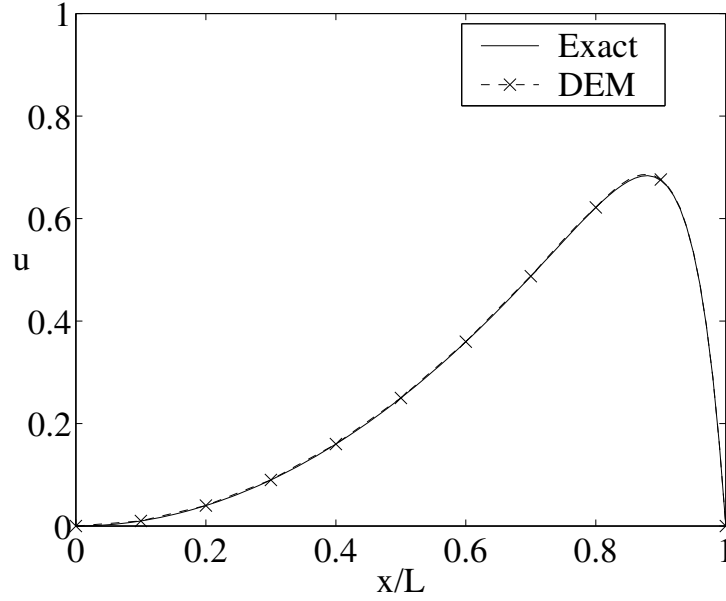
31

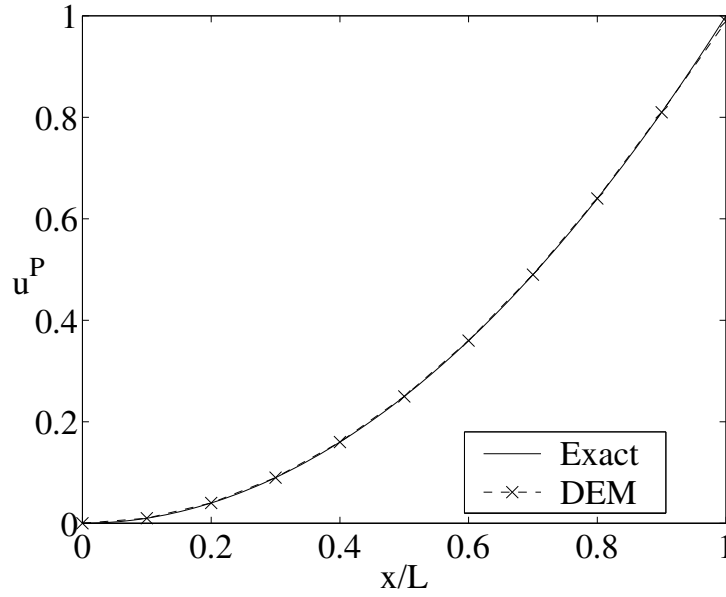Fig. 24. Inhomogeneous problem in one dimension, $\alpha = 1$.

Fig. 25. Particular solution of inhomogeneous problem and u^{P} in one dimension, $\alpha = 1$.

6 Conclusions

In this paper we present the discontinuous enrichment method, in which standard finite element polynomials are enriched by discontinuous functions. The enrichment within each element is spanned by free space solutions of the constant coefficient, homogeneous, partial differential equation that governs the problem that is being considered. Continuity across element boundaries and
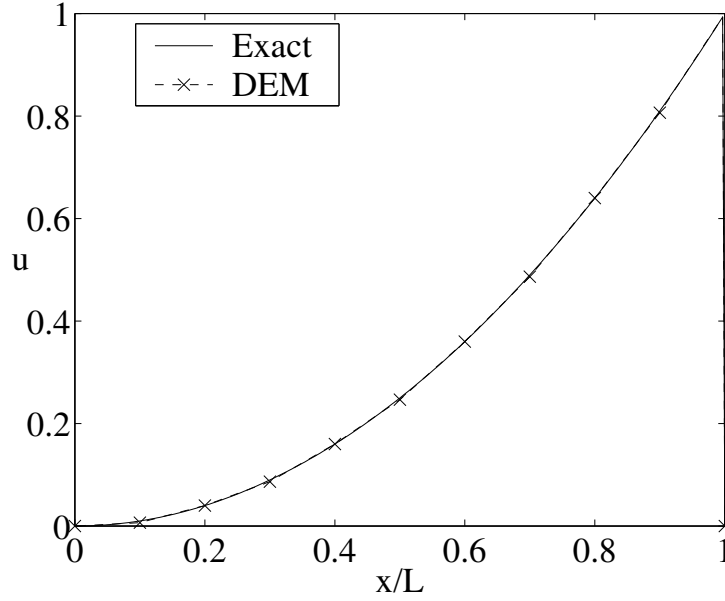
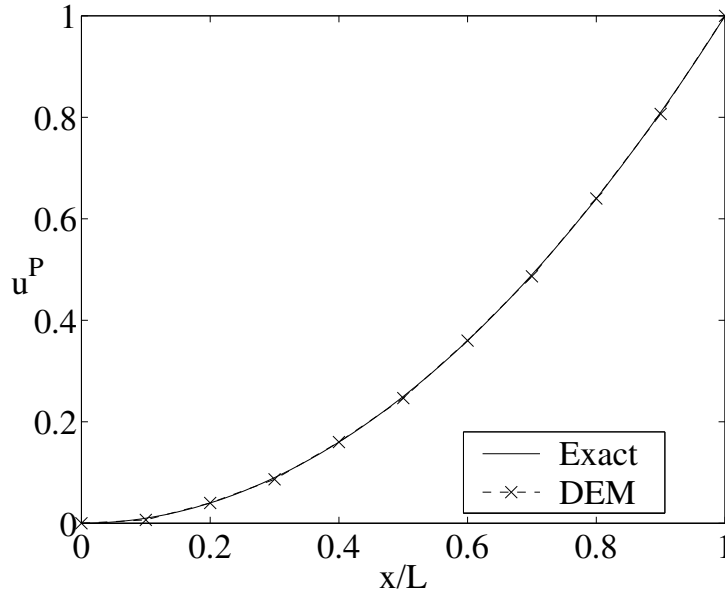Fig. 26. Inhomogeneous problem in one dimension, $\alpha = 10^6$.

Fig. 27. Particular solution of inhomogeneous problem and u^{P} in one dimension, $\alpha = 10^6$.

Dirichlet boundary conditions are enforced weakly by Lagrange multipliers. The Lagrange multipliers are taken as normal traces of a vector field on element boundaries, according to well-established procedures for hybrid methods.

Due to the discontinuous nature of the enrichment, it is eliminated from the formulation by static condensation on the element level, prior to assembly. Thus, the cost of solving the matrix problem that ensues from DEM is virtually independent of the dimension of the enrichment. Elimination of the enrichment

leads to a simpler formulation. The condensed problem is expressed in terms of the polynomial field and the Lagrange multipliers. The enrichment within each element is recovered after the solution as a post-processing step.

Examples of application of the proposed methodology to time-harmonic acoustics and advection-diffusion are presented. In the case of acoustics the enrichment is spanned by plane waves. The number of plane waves and their directions are determined in advance. In the two-dimensional implementation described herein, an underlying bilinear field is enriched by four plane waves aligned with the axes. The Lagrange multipliers have piecewise constant normal components on element boundaries. Dispersion analyses demonstrate the good performance of the DEM element. These properties are confirmed by accurate solutions on numerical tests, which also indicate adequate conditioning of the formulation.

An investigation of the application to advection-diffusion problems leads to similar conclusions. The enrichment in this case is spanned by a single exponential function in each element, so that element-level static condensation is a scalar operation. Preliminary numerical results are promising.

All indications in this work point to DEM as a cost effective computational choice for cases in which standard finite elements run into difficulties. We anticipate that for such problems, the proposed methodology can attain a given accuracy with the same order of conditioning as the standard Galerkin method, but at significantly lower cost.

Acknowledgment

References

[1] M. A. Aminpour, J. B. Ransom, and S. L. McCleary. Coupled analysis method for structures with independently modelled finite element subdomains. *Internat. J. Numer. Methods Engrg.*, 38(21):3695–3718, 1995.

[2] I. Babuška. The finite element method with Lagrangian multipliers. *Numer. Math.*, 20(3):179–192, 1973.

[3] I. Babuška, C. E. Baumann, and J. T. Oden. A discontinuous *hp* finite element method for diffusion problems: 1-D analysis. *Comput. Math. Appl.*, 37(9):103–122, 1999.

[4] I. Babuška, F. Ihlenburg, E. T. Paik, and S. A. Sauter. A generalized finite element method for solving the Helmholtz equation in two dimensions with minimal pollution. *Comput. Methods Appl. Mech. Engrg.*, 128(3-4):325–359, 1995.

[5] I. Babuška and J. M. Melenk. The partition of unity method. *Internat. J. Numer. Methods Engrg.*, 40(4):727–758, 1997.

[6] I. Babuška and S. A. Sauter. Is the pollution effect of the FEM avoidable for the Helmholtz equation considering high wave numbers? *SIAM J. Numer. Anal.*, 34(6):2392–2423, 1997.

[7] P. E. Barbone and I. Harari. Nearly H^1-optimal finite element methods. *Comput. Methods Appl. Mech. Engrg.*, 1999. Submitted.

[8] C. E. Baumann and J. T. Oden. A discontinuous hp finite element method for convection-diffusion problems. *Comput. Methods Appl. Mech. Engrg.*, 175(3-4):311–341, 1999.

[9] C. E. Baumann and J. T. Oden. A discontinuous hp finite element method for the Euler and Navier-Stokes equations. *Internat. J. Numer. Methods Fluids.*, 31(1):79–95, 1999.

[10] C. Bernardi, Y. Maday, and A. T. Patera. A new non conforming approach to domain decomposition: The mortar element method. In H. Brezis and J.-L. Lions, editors, *Nonlinear Partial Differential Equations and Their Applications. Collège de France Seminar, Vol. XI (Paris, 1989–1991)*, pages 13–51. Longman Sci. Tech., Harlow, 1994.

[11] P. Bettess, O. Laghrouche, J. Shirron, and B. Peseux. Semi-analytical integration rules for special wave finite elements. In *Proceedings of the Seventh International Congress on Sound and Vibration*, pages 2163–2170. IIAV, 2000.

[12] P. Bouillard. Influence of the pollution on the admissible field error estimation for FE solutions of the Helmholtz equation. *Internat. J. Numer. Methods Engrg.*, 45(7):783–800, 1999.

[13] F. Brezzi, J. Douglas, Jr., M. Fortin, and L. D. Marini. Efficient rectangular mixed finite elements in two and three space variables. *RAIRO Modél. Math. Anal. Numér.*, 21(4):581–604, 1987.

[14] F. Brezzi, J. Douglas, Jr., and L. D. Marini. Two families of mixed finite elements for second order elliptic problems. *Numer. Math.*, 47(2):217–235, 1985.

[15] F. Brezzi and M. Fortin. *Mixed and Hybrid Finite Element Methods*, volume 15 of *Springer Series in Computational Mathematics*. Springer-Verlag, New York, 1991.

[16] F. Brezzi, L. P. Franca, T. J. R. Hughes, and A. Russo. $b = \int g$. *Comput. Methods Appl. Mech. Engrg.*, 145(3-4):329–339, 1997.

[17] F. Brezzi, L. P. Franca, and A. Russo. Further considerations on residual-free bubbles for advective-diffusive equations. *Comput. Methods Appl. Mech. Engrg.*, 166(1-2):25–33, 1998.

[18] A. N. Brooks and T. J. R. Hughes. Streamline upwind/Petrov-Galerkin formulations for convection dominated flows with particular emphasis

on the incompressible Navier-Stokes equations. *Comput. Methods Appl. Mech. Engrg.*, 32(1-3):199–259, 1982. FENOMECH '81, Part I (Stuttgart, 1981).

[19] Y. K. Cheung, W. G. Jin, and O. C. Zienkiewicz. Solution of Helmholtz equation by Trefftz method. *Internat. J. Numer. Methods Engrg.*, 32(1):63–78, 1991.

[20] K.-C. Chung, G. A. Evans, and J. R. Webster. A method to generate generalized quadrature rules for oscillatory integrals. *Appl. Numer. Math.*, 34(1):85–93, 2000.

[21] J. L. Cipolla. Subgrid modeling in a Galerkin method for the Helmholtz equation. *Comput. Methods Appl. Mech. Engrg.*, 177(1-2):35–49, 1999.

[22] J. Douglas, Jr. and J. P. Wang. An absolutely stabilized finite element method for the Stokes problem. *Math. Comp.*, 52(186):495–508, 1989.

[23] G. A. Evans and J. R. Webster. A comparison of some methods for the evaluation of highly oscillatory integrals. *J. Comput. Appl. Math.*, 112(1-2):55–69, 1999.

[24] C. Farhat. A Lagrange multiplier based on divide and conquer finite element algorithm. *J. Comput. System Engng.*, 2(2/3):149–156, 1991.

[25] C. Farhat. A saddle-point principle domain decomposition method for the solution of solid mechanics problems. In D. E. Keyes, T. F. Chan, G. Meurant, J. S. Scroggs, and R. G. Voigt, editors, *Fifth International Symposium on Domain Decomposition Methods for Partial Differential Equations (Norfolk, VA, 1991)*, pages 271–292. Society for Industrial and Applied Mathematics (SIAM), Philadelphia, PA, 1992.

[26] C. Farhat and M. Géradin. Using a reduced number of Lagrange multipliers for assembling parallel incomplete field finite element approximations. *Comput. Methods Appl. Mech. Engrg.*, 97(3):333–354, 1992.

[27] C. Farhat and M. Géradin. On a component mode synthesis method and its application to incompatible substructures. *Comput. & Structures*, 51(5):449–473, 1994.

[28] C. Farhat, A. Macedo, and M. Lesoinne. A two-level domain decomposition method for the iterative solution of high frequency exterior Helmholtz problems. *Numer. Math.*, 85(2):283–308, 2000.

[29] C. Farhat, J. Mandel, and F.-X. Roux. Optimal convergence properties of the FETI domain decomposition method. *Comput. Methods Appl. Mech. Engrg.*, 115(3):367–388, 1994.

[30] C. Farhat, K. Pierson, and M. Lesoinne. The second generation of FETI methods and their application to the parallel solution of large-scale linear and geometrically nonlinear structural analysis problems. *Comput. Methods Appl. Mech. Engrg.*, 184(2-4):333–374, 2000.

[31] C. Farhat and F.-X. Roux. A method of finite element tearing and interconnecting and its parallel solution algorithm. *Internat. J. Numer. Methods Engrg.*, 32(6):1205–1227, 1991.

[32] L. P. Franca and C. Farhat. Bubble functions prompt unusual stabilized finite element methods. *Comput. Methods Appl. Mech. Engrg.*, 123(1-

4):299–308, 1995.

[33] L. P. Franca, C. Farhat, M. Lesoinne, and A. Russo. Unusual stabilized finite element methods and residual free bubbles. *Internat. J. Numer. Methods Fluids.*, 27(2):159–168, 1998.

[34] L. P. Franca, C. Farhat, A. P. Macedo, and M. Lesoinne. Residual-free bubbles for the Helmholtz equation. *Internat. J. Numer. Methods Engrg.*, 40(21):4003–4009, 1997.

[35] L. P. Franca, S. L. Frey, and T. J. R. Hughes. Stabilized finite element methods: I. Application to the advective-diffusive model. *Comput. Methods Appl. Mech. Engrg.*, 95(2):253–276, 1992.

[36] L. P. Franca and A. P. Macedo. A two-level finite element method and its application to the Helmholtz equation. *Internat. J. Numer. Methods Engrg.*, 43(1):23–32, 1998.

[37] L. P. Franca, A. Nesliturk, and M. Stynes. On the stability of residual-free bubbles for convection-diffusion problems and their approximation by a two-level finite element method. *Comput. Methods Appl. Mech. Engrg.*, 166(1-2):35–49, 1998.

[38] K. Gerdes and F. Ihlenburg. On the pollution effect in FE solutions of the 3D-Helmholtz equation. *Comput. Methods Appl. Mech. Engrg.*, 170(1-2):155–172, 1999.

[39] I. Harari. Reducing spurious dispersion, anisotropy and reflection in finite element analysis of time-harmonic acoustics. *Comput. Methods Appl. Mech. Engrg.*, 140(1-2):39–58, 1997.

[40] T. J. R. Hughes. Multiscale phenomena: Green's functions, the Dirichlet-to-Neumann formulation, subgrid scale models, bubbles and the origins of stabilized methods. *Comput. Methods Appl. Mech. Engrg.*, 127(1-4):387–401, 1995.

[41] T. J. R. Hughes, G. R. Feijóo, M. Luca, and Q. Jean-Baptiste. The variational multiscale method - a paradigm for computational mechanics. *Comput. Methods Appl. Mech. Engrg.*, 166(1-2):3–24, 1998.

[42] T. J. R. Hughes and L. P. Franca. A new finite element formulation for computational fluid dynamics: VII. The Stokes problem with various well-posed boundary conditions: Symmetric formulations that converge for all velocity/pressure spaces. *Comput. Methods Appl. Mech. Engrg.*, 65(1):85–96, 1987.

[43] T. J. R. Hughes, L. P. Franca, and G. M. Hulbert. A new finite element formulation for computational fluid dynamics: VIII. The Galerkin/least-squares method for advective-diffusive equations. *Comput. Methods Appl. Mech. Engrg.*, 73(2):173–189, 1989.

[44] T. J. R. Hughes and G. M. Hulbert. Space-time finite element methods for elastodynamics: Formulations and error estimates. *Comput. Methods Appl. Mech. Engrg.*, 66(3):339–363, 1988.

[45] F. Ihlenburg and I. Babuška. Solution of Helmholtz problems by knowledge-based FEM. *CAMES*, 4(3/4):397–415, 1997.

[46] J. Jirousek and A. Wróblewski. *T*-elements: State of the art and future

trends. *Arch. Comput. Methods Engrg.*, 3(4):323–434, 1996.

[47] O. Laghrouche and P. Bettess. Short wave modelling using special finite elements. *J. Comput. Acoust.*, 8(1):189–210, 2000.

[48] J.-L. Lions and E. Magenes. *Non-homogeneous Boundary Value Problems and Applications*, volume 1. Springer-Verlag, New York, 1972. Translated from the French by P. Kenneth, Die Grundlehren der mathematischen Wissenschaften, Band 181.

[49] J. M. Melenk and I. Babuška. The partition of unity method finite element method: Basic theory and applications. *Comput. Methods Appl. Mech. Engrg.*, 139(1-4):289–314, 1996.

[50] E. Oñate. Derivation of stabilized equations for numerical solution of advective-diffusive transport and fluid flow problems. *Comput. Methods Appl. Mech. Engrg.*, 151(1-2):233–265, 1998. Symposium on Advances in Computational Mechanics, Vol. 3 (Austin, TX, 1997).

[51] A. A. Oberai and P. M. Pinsky. A residual-based finite element method for the Helmholtz equation. *Internat. J. Numer. Methods Engrg.*, 1999. Accepted.

[52] J. T. Oden, I. Babuška, and C. E. Baumann. A discontinuous *hp* finite element method for diffusion problems. *J. Comput. Phys.*, 146(2):491–519, 1998.

[53] J. R. O'Leary and I. Harari. Finite element analysis of stiffened plates. *Comput. & Structures*, 21(5):973–985, 1985.

[54] P.-A. Raviart and J.-M. Thomas. Primal hybrid finite element methods for 2nd order elliptic equations. *Math. Comp.*, 31(138):391–413, 1977.

[55] J. C. Simo, P. Wriggers, and R. L. Taylor. A perturbed Lagrangian formulation for the finite element solution of contact problems. *Comput. Methods Appl. Mech. Engrg.*, 50(2):163–180, 1985.

[56] M. Stojek. Least-squares Trefftz-type elements for the Helmholtz equation. *Internat. J. Numer. Methods Engrg.*, 41(5):831–849, 1998.

[57] R. Temam. *Navier-Stokes Equations*. North-Holland Publishing Co., Amsterdam, third edition, 1984. Theory and numerical analysis, With an appendix by F. Thomasset.

Contact author:

Charbel Farhat
Department of Aerospace Engineering Sciences
University of Colorado at Boulder
Boulder, CO 80309-0429, USA

tel: +1-303/492-3992
fax: +1-303/492-4990
e-mail: charbel.farhat@colorado.edu